WTM-261 July 1957

Technical Report

ON THE INTERACTION EFFECTS PRODUCED BY A JET EXHAUSTING LATERALLY NEAR THE TAIL OF AN OGIVE-CYLINDER MODEL IN A SUPERSONIC MAIN STREAM

P. W. Vinson
J. L. Amick
H. P. Liepman

Supersonic Wind Tunnel
Department of Aeronautical Engineering
University of Michigan
Ann Arbor

Engineering Research Institute Project No. 2470
Contract No. NAw-6466
NATIONAL ADVISORY COMMITTEE FOR AERONAUTICS

ABSTRACT

The experimentally determined interaction effects of a side-jet exhausting near the tail of an ogive-cylinder model are presented and discussed. The interaction force is found to be independent of main stream Mach number, boundary layer condition (laminar vs. turbulent), angle of attack, and forebody length. The ratio of interaction force to jet force is found to be inversely proportional to the square root of the product of jet stagnation-to-free stream pressure ratio and jet-to-body diameter ratio.

OBJECTIVE

The purpose of the investigation was to provide experimental data on the aerodynamic effects of a jet exhausting laterally near the base of a slender body of revolution in a supersonic main stream.

INTRODUCTION

One attractive method of controlling the flight path or attitude of a space vehicle is by means of gas jets directed normal to the body axis. Since such side-jets could also give useful control forces during atmospheric flight, the interaction of a side-jet with a supersonic flow is of interest. This report presents the results of a continuing investigation of these interaction effects.

References 1 and 2 contain results of investigations of the interaction effects of a side-jet issuing near the center of gravity of a cone-cylinder model. The results of these investigations indicated that the interaction effects were negligible but it was noted that the interaction effects need not be small for other jet locations. The present investigation was undertaken to determine the magnitude of the interaction effects

of a side-jet issuing near the tail of an ogive-cylinder model.

Data on the interaction force were obtained by measuring, with a sting balance, the normal force due to a side-jet discharging into a supersonic main stream and into a vacuum. Comparison of these two cases gave the interaction force. Interaction forces were measured for: laminar and turbulent boundary layers; model forebody lengths of 3.4 and 5.4 body diameters; angles of attack from -12° to +14°; various afterbody lengths from .0625 to 0.625 body diameters; main stream Mach numbers of 2.84 and 3.90; circular jet orifices of 0.159 and 0.221 inches diameter; and jet stagnation-to-free stream static pressure ratios of 10 to 900. Schlieren photographs were obtained of representative runs to aid in a qualitative analysis of the interaction effects. Base pressure measurements were made to determine the effect of the side-jet on model drag for both laminar and turbulent boundary layers.

This work was conducted at the Supersonic Wind Tunnel, Department of Aeronautical Engineering, University of Michigan, under the sponsorship and with the financial assistance of the National Advisory Committee for Aeronautics.

SYMBOLS

a	speed of sound
A_j	cross sectional area of jet orifice
A_m	cross sectional area of model
d	diameter of jet orifice
D	diameter of model
ℓ	distance from center of jet orifice to model base
L	distance from model nose to center of jet orifice
M	Mach number
N_Δ	normal force increment due to jet (normal force on model in main

stream with jet on, minus normal force due to main stream alone at same angle of attack)

N_I interaction force (N_Δ minus N_V)

N_V normal force due to jet exhausting into a vacuum

N_{Vt} theoretical value of N_V $2\left(\frac{2}{\gamma+1}\right)^{\frac{1}{\gamma+1}} p_{oj} A_j$

p pressure

R_e Reynolds number

T temperature

V velocity

X location of line of action normal force from center of jet orifice

α angle of attack

δ angle through which main stream ahead of side-jet is turned

γ ratio of specific heats of the jet gas

μ viscosity

ρ density

Subscript:

0 stagnation conditions

1 free stream conditions

b model base conditions

j jet conditions

Superscript:

* conditions at M = 1

THEORETICAL METHODS

In attempting to provide a theoretical basis for the observed interaction effects, an analysis of a two-dimensional isentropic jet expansion has been made. The jet is assumed to expand isentropically, separating the

boundary layer, and causing the main flow to turn through an angle δ upstream of the jet. (See sketch (a).)

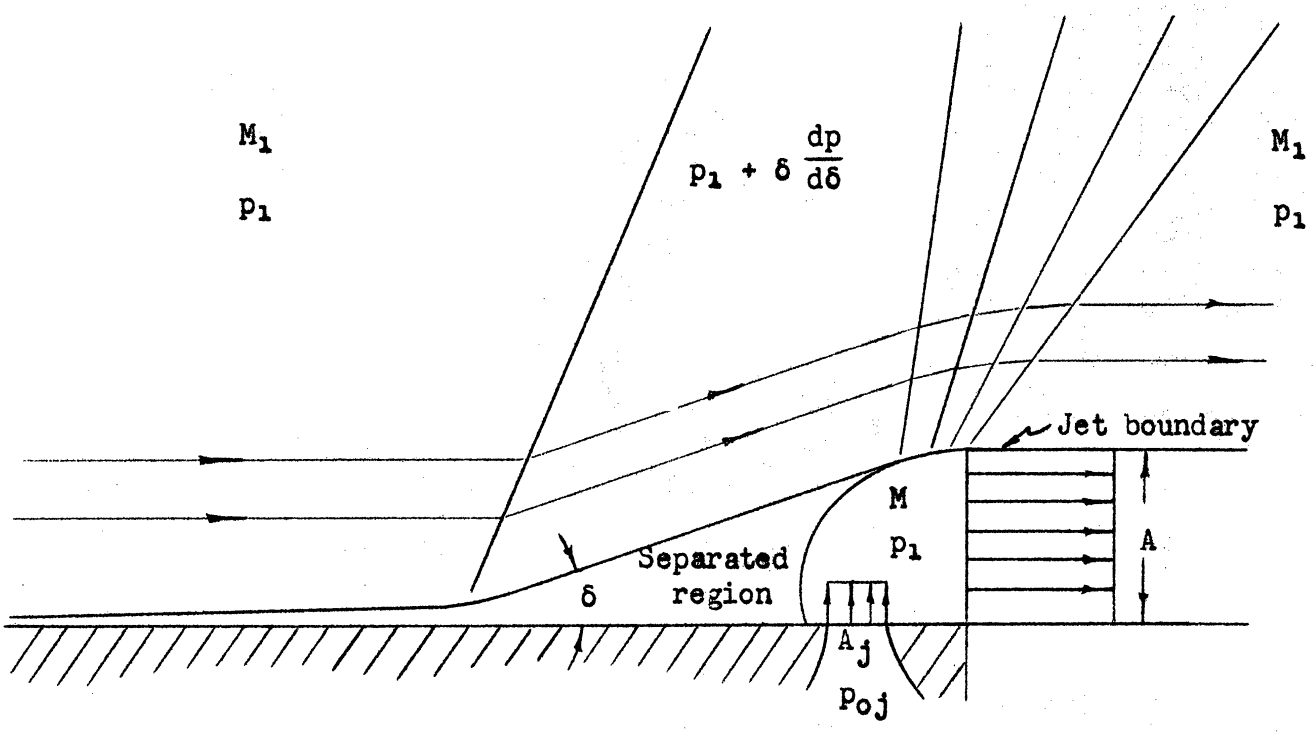

Sketch (a)

Assuming that no diffusion occurs across the jet boundary and that sonic conditions exist at the throat of the jet orifice, conservation of jet mass flow requires that

$$\frac{A}{A_j} = \left(\frac{2}{\gamma+1}\right)^{\frac{\gamma+1}{2(\gamma-1)}} \frac{\left(1 + \frac{\gamma-1}{2} M^2\right)^{\frac{\gamma+1}{2(\gamma-1)}}}{M}$$

Mach number is related to total-to-static pressure ratio by the equation

$$\frac{p_{oj}}{p_1} = \left(1 + \frac{\gamma-1}{2} M^2\right)^{\frac{\gamma}{\gamma-1}}$$

Combining these two equations provides an expression for the area ratio, A/A_j, in terms of the pressure ratio, p_{oj}/p_1

$$\frac{A}{A_j} = \left(\frac{2}{\gamma+1}\right)^{\frac{\gamma+1}{2(\gamma-1)}} \frac{\left(\frac{p_{oj}}{p_1}\right)^{\frac{\gamma+1}{2\gamma}}}{\sqrt{\frac{2}{\gamma-1}\left[\left(\frac{p_{oj}}{p_1}\right)^{\frac{\gamma-1}{\gamma}} - 1\right]}}$$

The theoretical interaction force is equal to the unbalanced pressure in the separated region times the area exposed to separation.

$$N_{It} = \left(p_1 + \delta \frac{dp}{d\delta} - p_1\right) \frac{A}{\tan \delta}$$

For small angles the tangent approximates the angle and

$$N_{It} = A \frac{dp}{d\delta}$$

The ratio of theoretical interaction force to theoretical jet force is

$$\frac{N_{It}}{N_{Vt}} = \frac{A \frac{dp}{d\delta}}{2\left(\frac{2}{\gamma+1}\right)^{\frac{1}{\gamma-1}} p_{oj} A_j}$$

Substitution for the area ratio, A/A_j, yields an expression for N_{It}/N_{Vt} in terms of p_{oj}/p_1

$$\frac{N_{It}}{N_{Vt}} = \frac{1}{2}\left(\frac{2}{\gamma+1}\right)^{\frac{1}{2}} \frac{\frac{d(p/p_1)}{d\delta}}{\left(\frac{p_{oj}}{p_1}\right)^{\frac{\gamma-1}{2\gamma}}\left[\frac{2}{\gamma-1}\left\{\left(\frac{p_{oj}}{p_1}\right)^{\frac{\gamma-1}{\gamma}} - 1\right\}\right]^{\frac{1}{2}}}$$

The two-dimensional theory then indicates that pressure ratio, p_{oj}/p_1, jet gas specific heat ratio, γ , and rate of change of static pressure ratio with flow deflection angle, $d(p/p_1)/d\delta$, are the important parameters

controlling the interaction effects. Since $d(p/p_1)/d\delta$ increases slightly with Mach number, the interaction effects should increase with Mach number.

Figure 1 is a plot of the two-dimensional theory and shows the predicted interaction force for an air jet ($\gamma = 1.4$), exhaust gases ($\gamma = 1.2$), and monatomic gases ($\gamma = 1.67$).

EXPERIMENTAL TECHNIQUES

Apparatus

The present data were obtained in the University of Michigan 8- by 13-inch Supersonic Wind Tunnel utilizing the Mach 2.84 and Mach 3.90 nozzle blocks. This tunnel is of the intermittent blowdown-from-atmospheric-pressure type with run times of up to 20 seconds. The Reynolds number at Mach 2.84 is about $.20 \times 10^6$ per inch and at Mach 3.90 is about $.13 \times 10^6$ per inch. Calibration of the flow produced by the Mach 2.84 and Mach 3.90 nozzle blocks is reported in References 3 and 4.

Jet air pressures above atmospheric were obtained from the shop air line at a pressure of approximately 90 psig. Two Grove regulators were installed in parallel in the jet air line to provide pressure regulation and a manually operated plug valve, downstream of the regulators, provided on-off control of air flow to the model.

Jet air pressures less than atmospheric were obtained by breaking the air supply line upstream of the plug valve. Atmospheric air was then throttled to the desired pressure by partially closing the plug valve.

The shop air was contaminated with a certain amount of entrained oil. The effect of oil contamination was considered negligible since there were no discernable differences between the atmospheric and shop air data. The only apparent effect was to cause oil streaks on the tunnel window toward which the jet was directed for some of the schlieren photographs.

Normal force data were obtained from two 4-element strain gage bridges mounted on flats milled in a hollow steel sting which also served as the supply line for jet air. A multi-channel, bridge type, amplifier provided strain gage excitation and amplified the output signal sufficiently to drive a sensitive oscillograph galvanometer. Test data were recorded on photographic paper for subsequent reduction. Calibration data were obtained after each series of runs by hanging weights on the end of the sting and recording galvanometer deflections.

A pitot tube and thermocouple were located inside the sting near the jet orifice providing jet stagnation pressure and temperature data. The thermocouple output was sufficient to drive a galvanometer without intermediate amplification. Jet stagnation pressures greater than atmospheric were read directly on a pressure gage while sub-atmospheric pressures were read on a mercury manometer.

Models

The models tested consisted of various combinations of the components shown in Figure 2. The base, containing the jet orifice, had internal threads for attachment to the hollow sting and an "O" ring to prevent jet air leakage. The two forebodies shown were attached to the front of the base also by means of threads and an "O" ring seal. The spacers were attached to the base in various combinations to give the desired afterbody lengths.

Each of the two forebodies had an approximately ogive-shaped nose three diameters long followed by a two-inch diameter cylinder. When mounted on the base they gave nose-to-orifice distances, L, of 3.4 and 5.4 diameters.

Two different jet orifice diameters were tested. After tests had been made on the smaller diameter orifice, d = .159 inches, the orifice was plugged and a larger orifice, .221 inches in diameter, was drilled in the opposite side of the base. Views of the assembled model showing the two orifice sizes

appear in Figure 3. The short forebody (L/D = 3.4) is shown attached to the base with the complete set of afterbody spacers. The ring shown on the nose of the model was used to provide a turbulent boundary layer for some of the tests.

Details of the internal orifice geometry are shown in sketch (b).

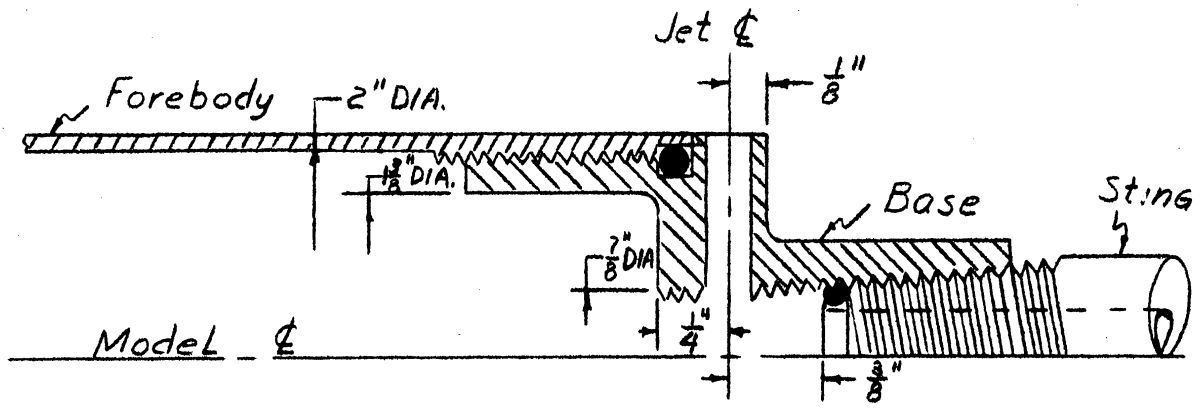

Sketch (b)

Both orifices tested entered the base in the portion threaded for sting attachment. The actual orifice entry details then varied somewhat for the two orifices tested.

The complete model-sting assembly is shown in Figure 4.

Tests

Jet tare force calibrations were obtained by evacuating the test section to approximately 2 inches of mercury absolute pressure, and shielding the model externally against the jet blast. By this method the effects of external pressure distribution were eliminated and data on the variation of the measured jet force, N_V, with jet stagnation pressure, were obtained. Figure 5 shows the observed variation of N_V/N_{Vt} with jet stagnation pressure for the two orifices tested. The difference in level of the two curves is probably due to the different orifice entrance conditions as shown in sketch (b) above. Earlier tests without model shielding indicated a 6% loss in measured jet force due to the external pressure field.

Tests were made at Mach 2.84 with the long forebody (L/D = 5.4) and a laminar boundary layer, but china clay patterns of the boundary layer separation were irregular and unsymmetrical, indicating an unstable laminar boundary layer. This boundary layer instability was attributed to interaction of tunnel disturbances with the model, and subsequent runs were made with the boundary layer trip on the model nose. Data on the variation of the interaction force with jet stagnation pressure, angle of attack, and afterbody length were obtained for the long forebody-turbulent boundary layer model.

China clay patterns of the boundary layer separation at Mach 2.84 on the short forebody (L/D = 3.4) indicated a stable laminar boundary layer, and data were obtained for both laminar and turbulent boundary layers. In addition, data were obtained for two orifice diameters (.159 and .221 inches) and for various afterbody lengths.

At Mach 3.9, it was found that a stable laminar boundary layer existed on both the short and long models. Consequently, data were obtained for both models with laminar and turbulent boundary layers. Unfortunately, an amplifier maladjustment rendered the bulk of the Mach 3.9 data invalid. It is felt that the long forebody, turbulent boundary layer data is valid, but caution should be used in applying this data since there is some question as to its validity.

During the initial test phase, base pressure readings were obtained by measuring the pressure inside the windshield. However, the windshield was found to change the nature of the jet effect on base pressure. Therefore the remainder of the testing was done without base pressure measurements except for one series of runs with the windshield removed. No attempt was made to obtain normal force data for the "windshield removed" runs.

Accuracy

An analysis of the probable errors in measuring normal force magnitudes

predicts a maximum probable error of ±15% of N_I/N_V. The bulk of the experimental data falls within this predicted range of accuracy.

RESULTS AND DISCUSSION

Normal Force Data

Data on the normal force due to jet interaction, N_I, are presented in Figures 6 through 14, covering the parameters varied in this investigation. Reference 1 contains a dimensional analysis of the parameters involved in the jet-main flow interaction which indicates that p_{oj}/p_1, d/D, and A_j/A_m, among others, may be important dimensionless quantities governing the interaction effects. The two-dimensional theoretical approach presented in this report indicates that only p_{oj}/p_1 should be important for correlation of N_I/N_V data. It is natural to expect that a ratio of characteristic jet dimension-to-body dimension should be important in three-dimensional flow. Verification of the importance of the parameter $p_{oj}\, d/p_1 D$ is shown in Figure 8. Good correlation of N_I/N_V data is obtained, for the two diameter jet orifices tested, using the dimensionless parameter $p_{oj}\, d/p_1 D$.

Within the limits of accuracy of the present data, main stream Mach number, boundary layer condition (laminar or turbulent), and L/D ratio are found to have a negligible effect upon the interaction force. While most of the angle of attack data fall within the predicted accuracy range, there is a definite trend of increased interaction force at negative angles of attack, and reduced interaction force at positive angles. An empirical equation

$$\frac{N_I}{N_V} = \frac{.92}{\left[\frac{p_{oj}\, d}{p_1 D}\right]^{1/2}}$$

fits the experimental curve of Figure 6, which contains all of the experimental data with minimum afterbody length ($\ell/D = .0625$).

Figure 13 contains data for various afterbody length to body diameter ratios, ℓ/D, from .0625 to .625. While the data again does not greatly exceed the predicted range of accuracy, there is a consistent reduction in interaction force with increasing afterbody length.

Since the two-dimensional theory does not depend upon the jet orifice-to-body diameter ratio, as does the experimental data, a direct comparison cannot be made. Figure 7 shows the two-dimensional theory plotted with the data for the two orifice diameters tested. Obviously the agreement of experiment with theory is dependent upon the diameter ratio and Mach number selected. However, it is important to note that the two-dimensional theory does correctly predict the reduction in interaction force with increasing pressure ratio.

Resultant normal force location data are shown in Figure 14. These data cannot be correlated, but the location of the normal force, on an average, does not exceed .05 body diameters from the center of the jet orifice. Thus, for all practical purposes, the normal force can be assumed to act at the center of the jet orifice.

Base Pressure Data

Figure 15 shows the result of a circumferential base pressure survey with the windshield removed. No attempt was made to measure radial pressure variations. The circumferential survey indicates existence of a low pressure region directly behind the jet and a high pressure region in the wake opposite the jet orifice. An integrated average pressure reading occurs at a point 90° from the jet orifice. The "windshield removed" data of Figure 16 was obtained at the 90° location. The effect of the windshield on base pressure is apparent. No attempt was made to evaluate the effect of the presence of the sting on base pressure, although this effect is probably considerable, since the sting diameter is approximately one-half that of the model. Base

pressure decreases with the windshield removed and the jet on, indicating a rise in model drag due to the jet. This decrease in base pressure due to the jet is slightly greater for a laminar boundary layer than for a turbulent boundary layer, as might be expected.

Schlieren Photographs and China Clay Patterns

The schlieren photographs in Figures 17 through 22 give a qualitative picture of the effect of the different parameters on interaction force. They, together with the china clay patterns, Figure 23, provide a possible explanation for the negligible effect of boundary layer condition on interaction force. The laminar boundary layer separation covers a larger area of the model than the turbulent separation, but the pressure rise at separation is greater for turbulent boundary layer than for a laminar boundary layer. These two effects are in opposition and probably explain the negligible effect of boundary layer condition on interaction force. This experimental result is in agreement with the two-dimensional isentropic theory presented earlier, which says that the two effects are equal and cancel each other.

Combination of the spreading effect of the jet region-of-influence and the low pressure region directly behind the jet probably accounts for the reduced interaction force with increasing afterbody length.

Jet Efficiency

Since the interaction force, N_I, becomes an increasingly smaller percentage of the jet force, N_V, as pressure-diameter ratio parameter, $p_{o_j} d/p_1 D$, is increased, it is desirable to design for small values of this parameter in order to make the most efficient use of the jet. This can be accomplished, for a given total normal force, by using a large value of d/D and a small value of p_{o_j}/p_1. The advantage of a larger jet diameter is shown in Figure 24, where normal force is plotted as a function of the jet thrust in a vacuum, N_V. Since the jet mass flow is proportional to N_V, it is apparent that the

larger jet would require less mass flow to produce a given normal force.

The jet should be located as near the tail as possible to minimize the loss in interaction force due to spreading of the jet region-of-influence. This is particularly desirable for a laminar boundary layer where the jet spreading action is more pronounced. The desirability of having the jet near the tail is fortunate since it also reduces the body area exposed to corrosive exhaust gases, should they be used as the jet medium.

CONCLUSIONS AND RECOMMENDATIONS

The interaction force for the present investigation is found to be favorable, and to be independent of main stream Mach number, boundary layer condition, and forebody length, while angle of attack has only a secondary effect. For an air jet located close to the base, the ratio of interaction force to jet thrust is $N_I/N_V = .92/\sqrt{p_{o_j}\, d/p_1 D}$. Increasing the body length behind the jet decreases the interaction force somewhat. A small direct drag is associated with the side-jet in the form of a decrease in base pressure.

It is recommended that further investigations to determine, in detail, the flow field in the vicinity of a side-jet, be made. Pressure measurements over the body in the vicinity of the side-jet should provide a basis for understanding the mechanism of jet-main stream interaction. The predicted effect of utilizing exhaust gases should also be verified experimentally.

REFERENCES

1. Morkovin, M. V., Pierce, C. A. Jr., and Craven, C. E., "Interaction of a Side-Jet with a Supersonic Main Stream," Engineering Research Bulletin No. 35, University of Michigan, 1952.

2. Amick, J. L., Bond, C. E., and Liepman, H. P., "An Experimental Investigation of the Forces and Flow Fields Produced by a Jet Exhausting Laterally from a Cone-Cylinder in a Mach 2.84 Stream," WTM-255, University of Michigan, 1955.

3. Culbertson, P. E., "Calibration Report on the University of Michigan Supersonic Wind Tunnel," Parts III and IV, WTM-213, University of Michigan, 1952.

4. Murphy, J. C., and Sivier, K. R., "Progress Report on Mach 4 Nozzle Calibration," WTM-199, University of Michigan, 1951.

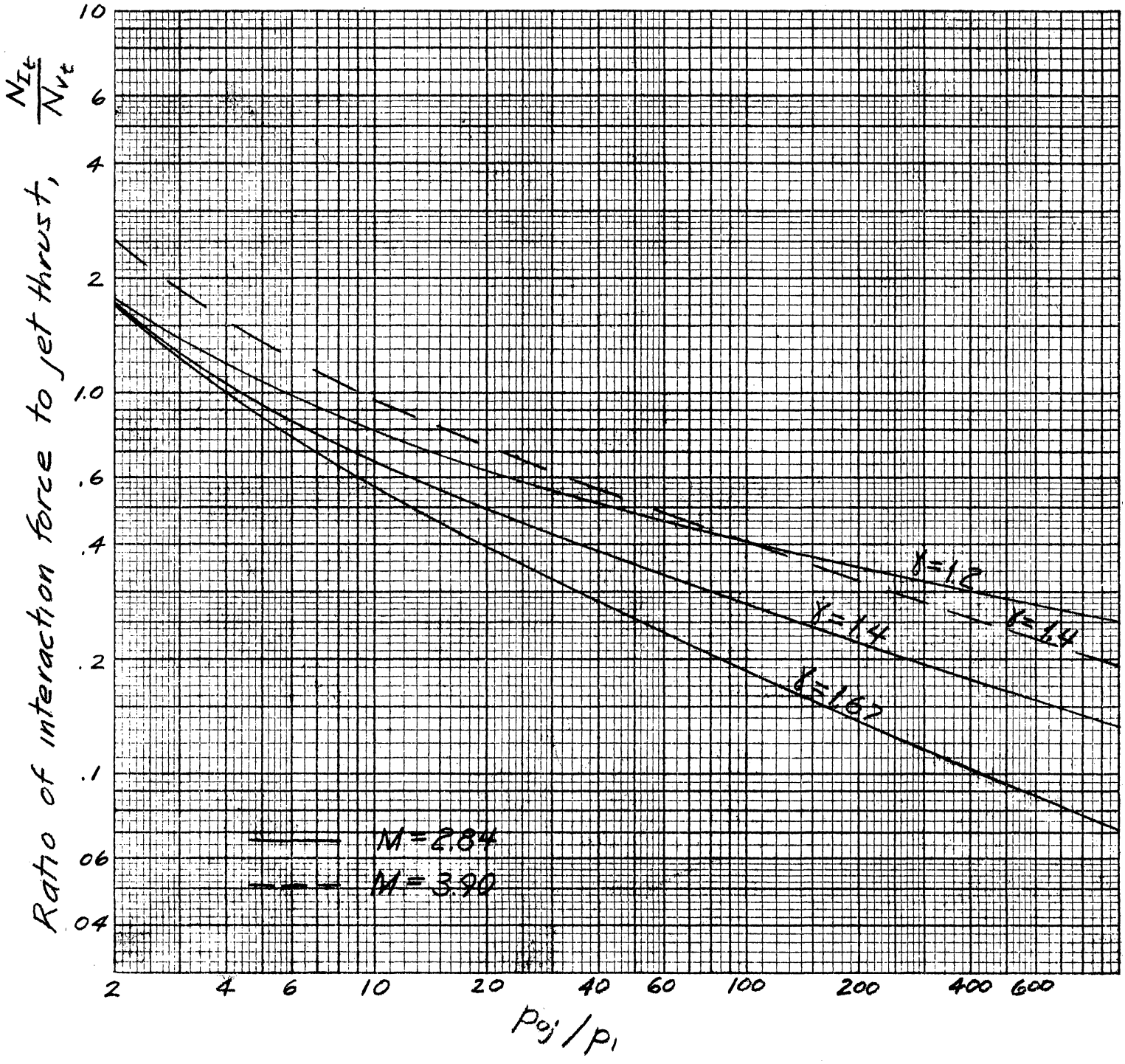

Figure 1. Two-dimensional isentropic theory.

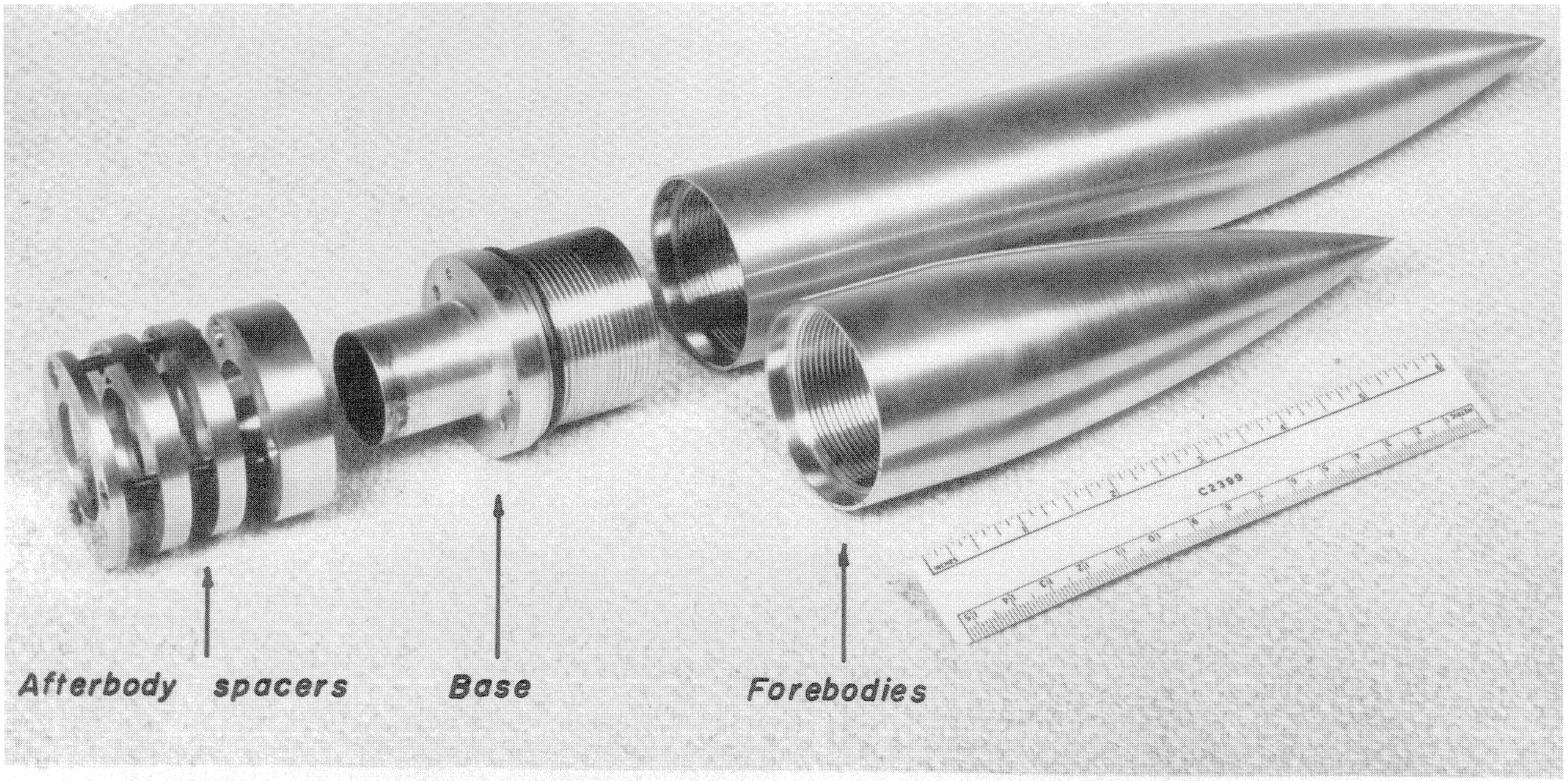

Figure 2 Exploded view of side-jet model

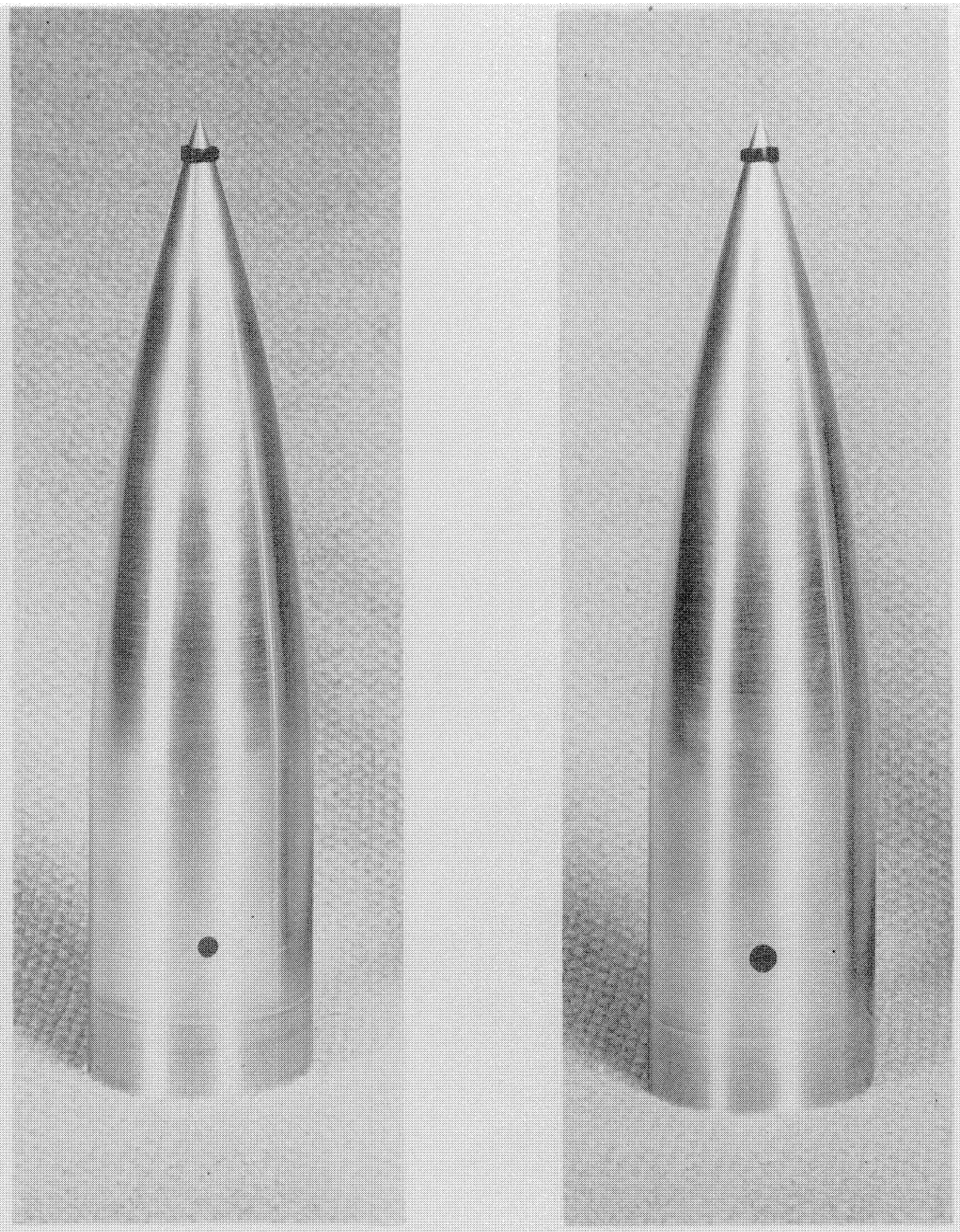

d = .159

d = .221

Figure 3 Side-jet model (L/D= 3.4), afterbody spacers and boundary layer trip attached

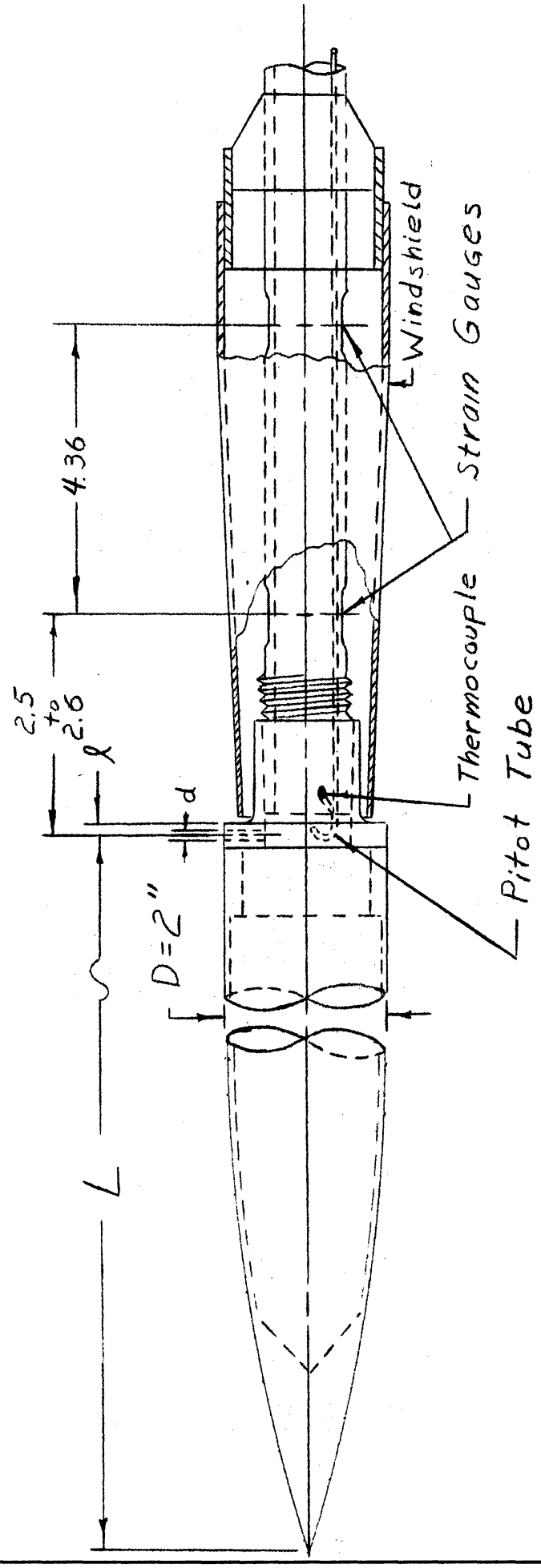

Figure 4. Model - sting assembly.

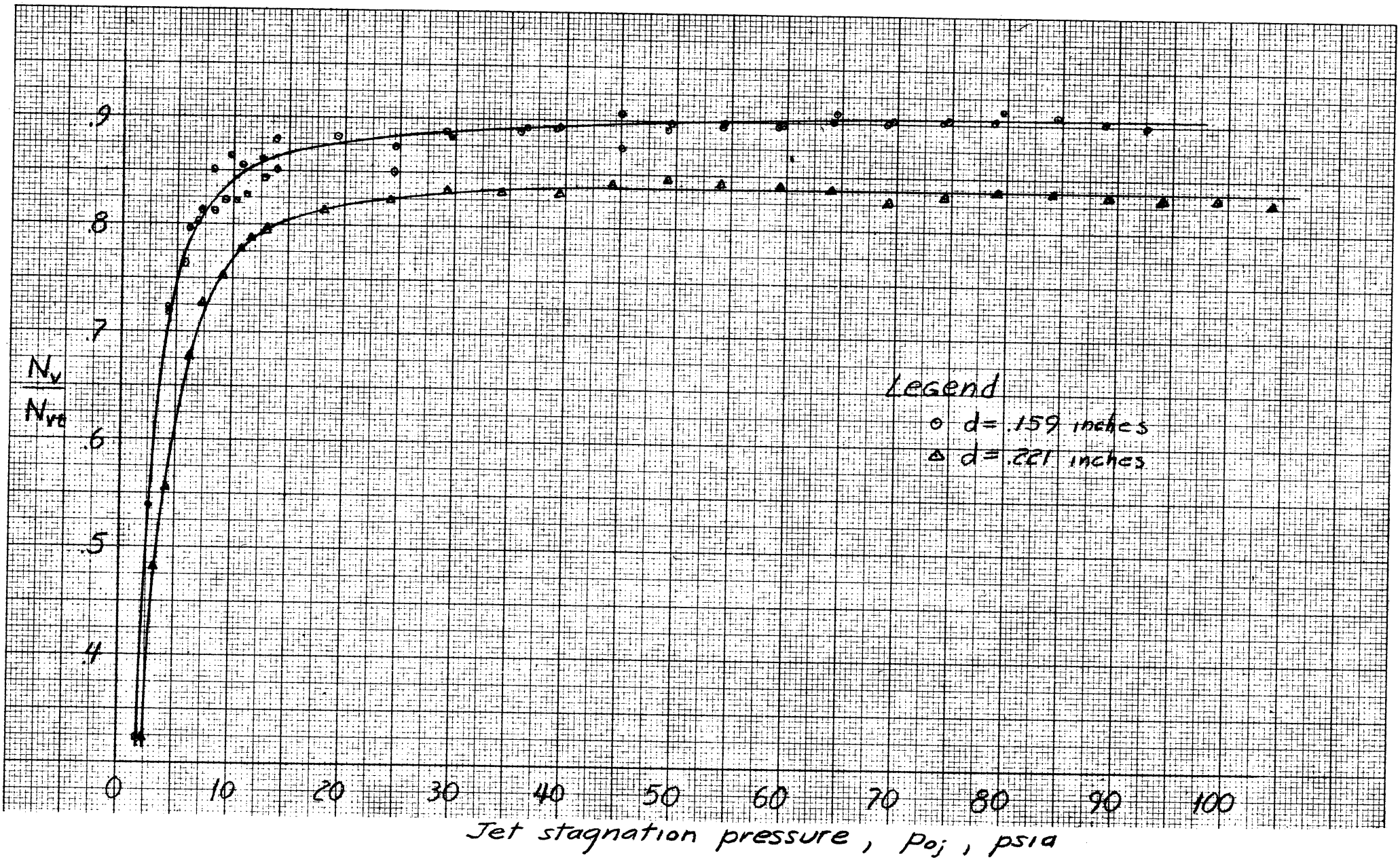

Figure 5. Jet tare force calibration. Jet exhausting into a vacuum, model shielded externally.

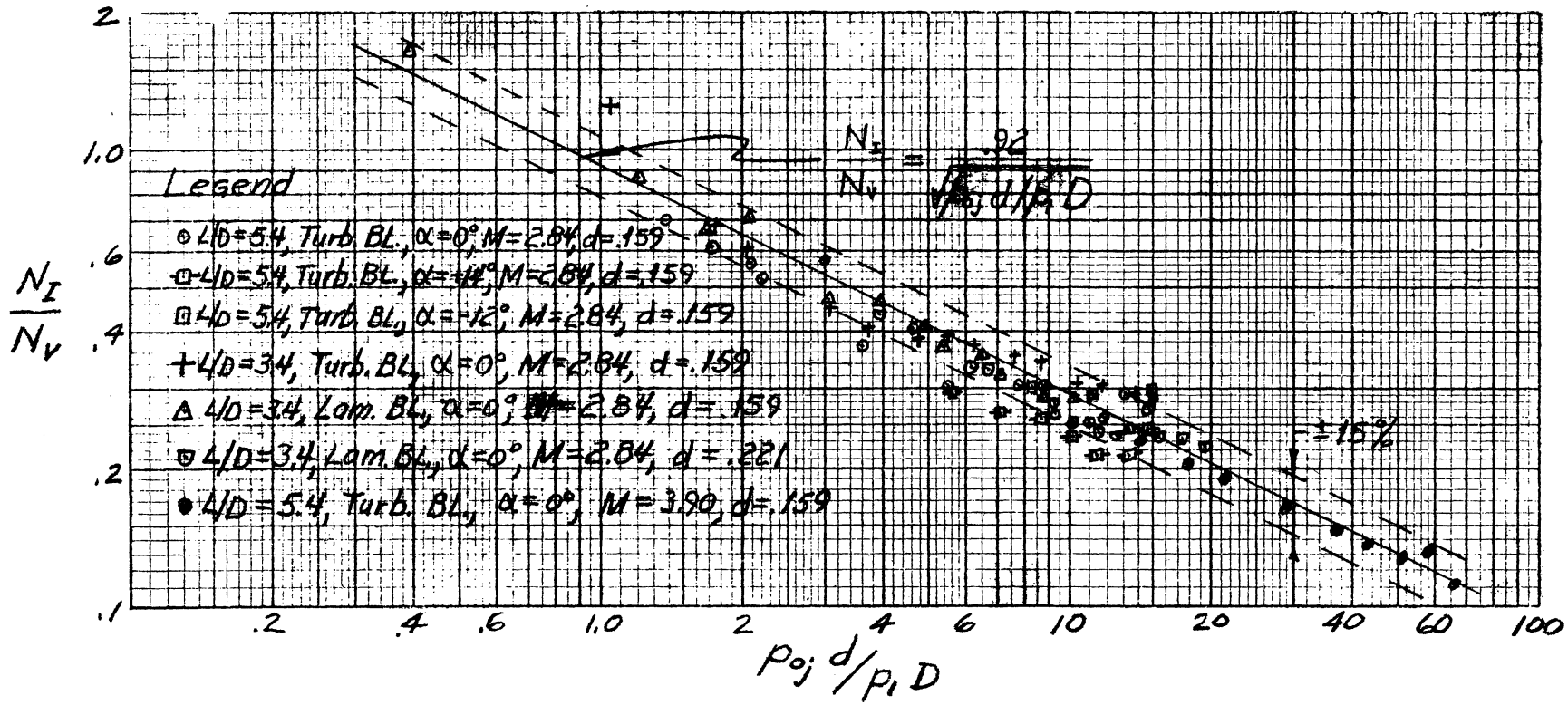

Figure 6. Correlation of experimental data. $\ell/D = .0625$.

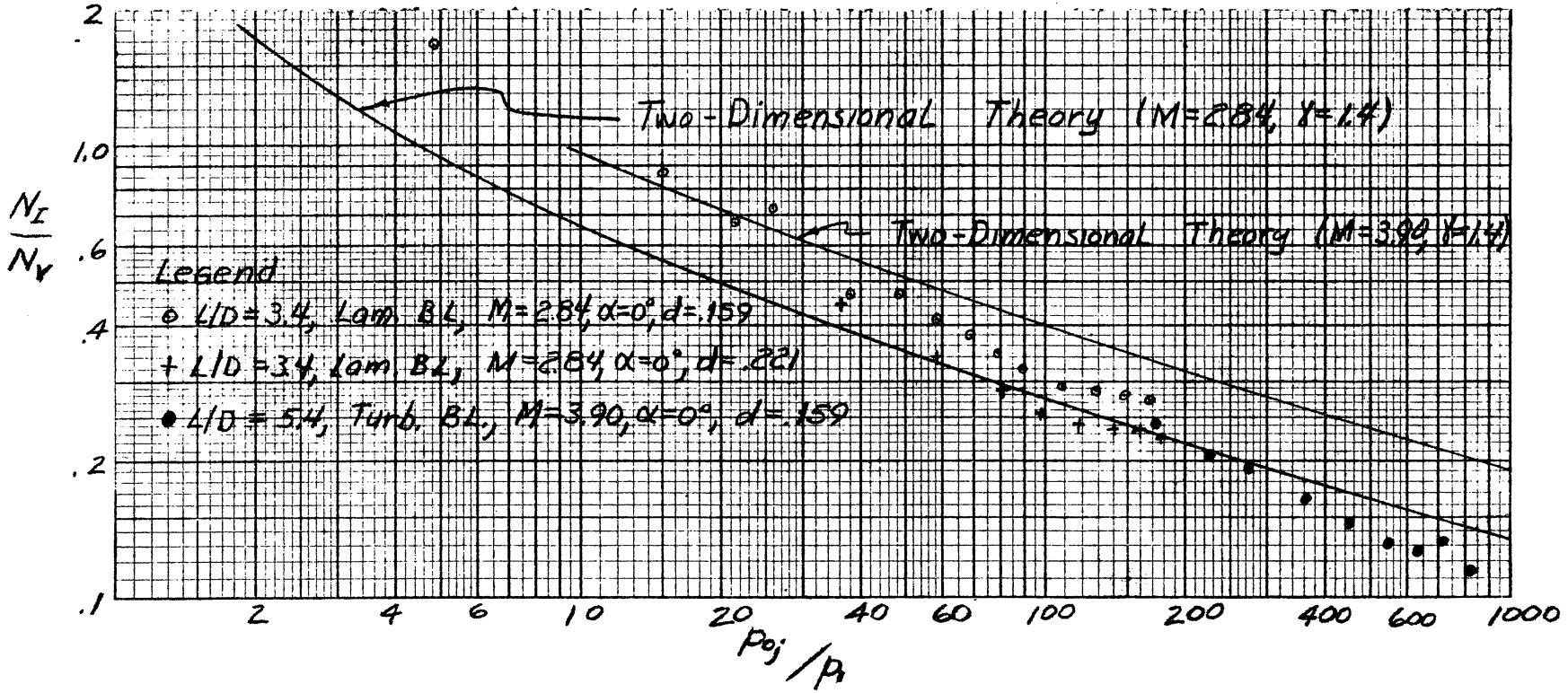

Figure 7. Comparison of experimental data with two-dimensional theory. $\ell/D = .0625$.

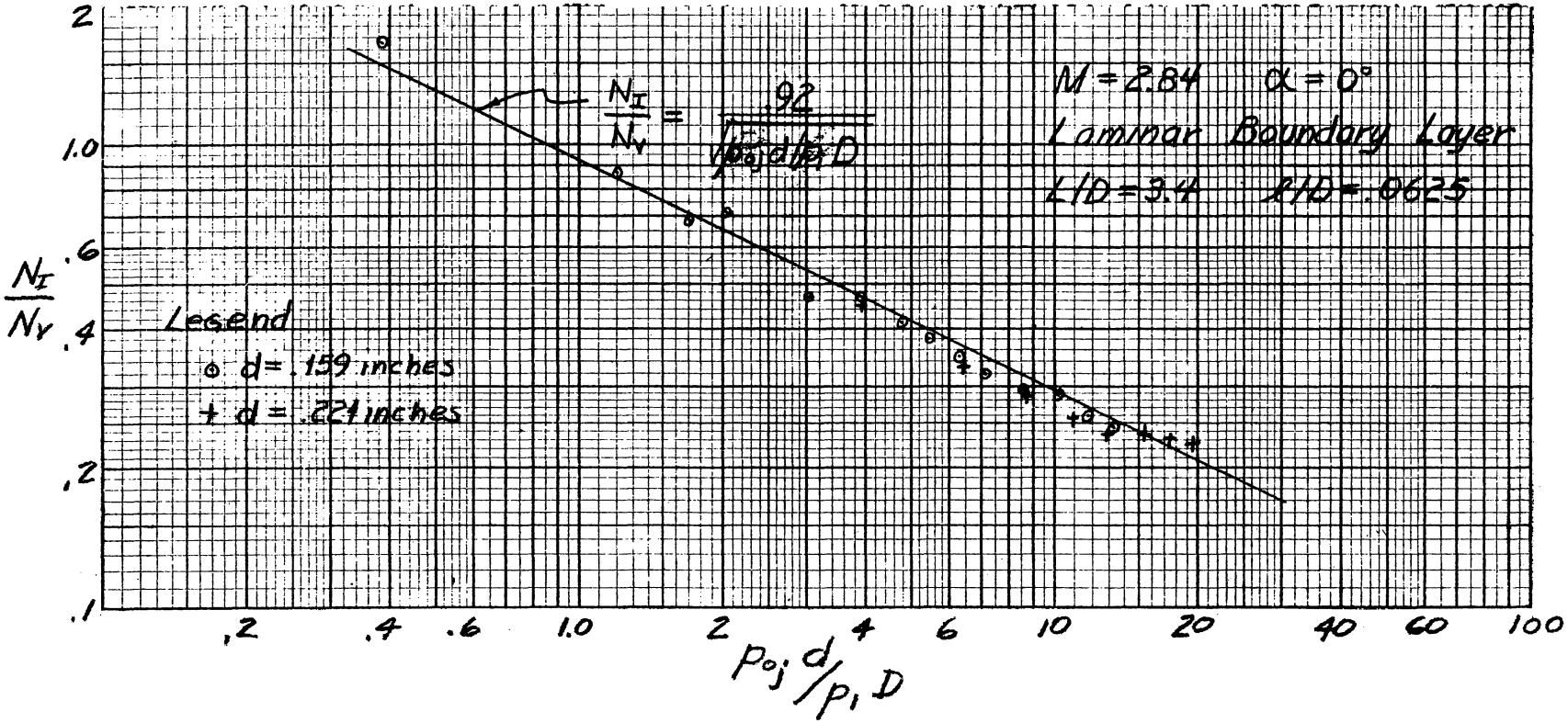

Figure 8. Effect of jet orifice diameter on interaction force.

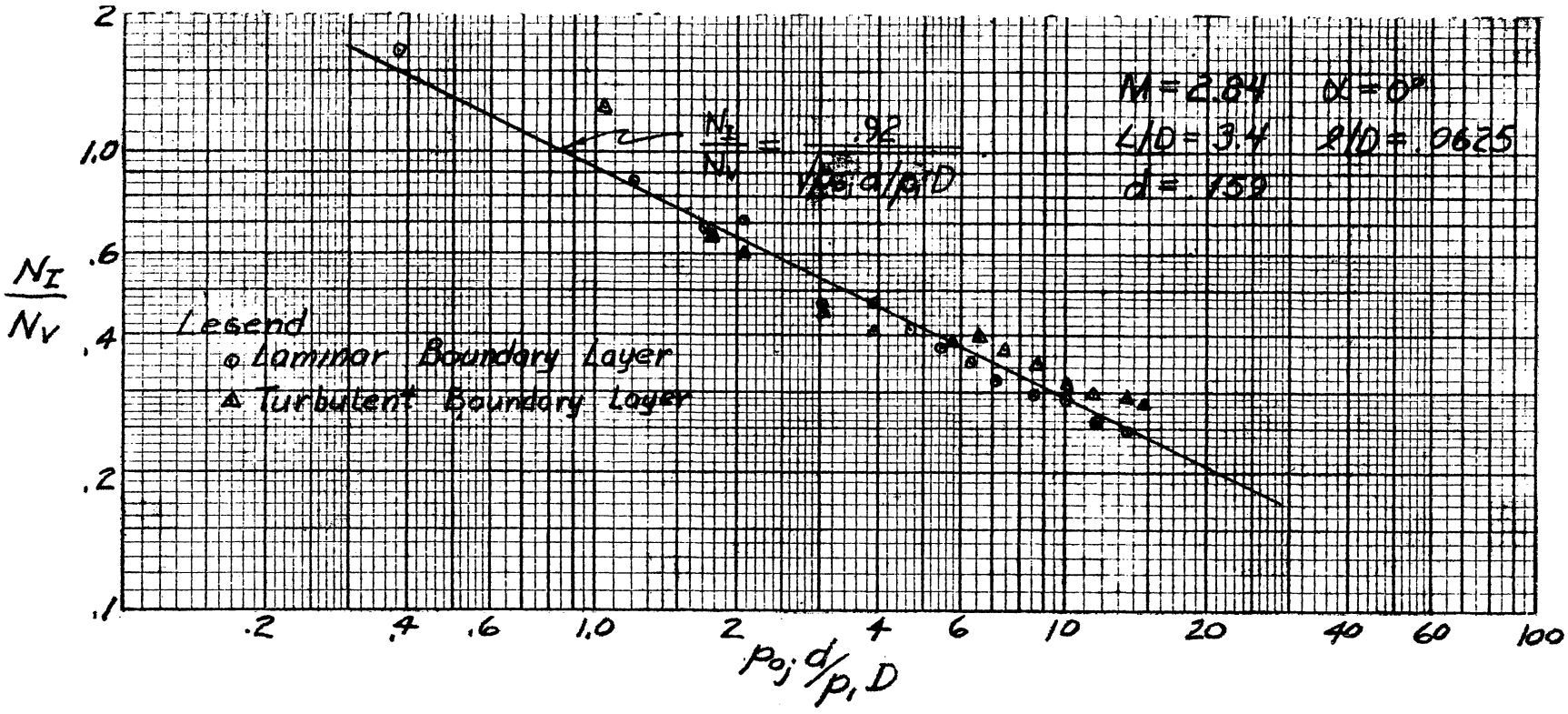

Figure 9. Effect of boundary layer condition on interaction force.

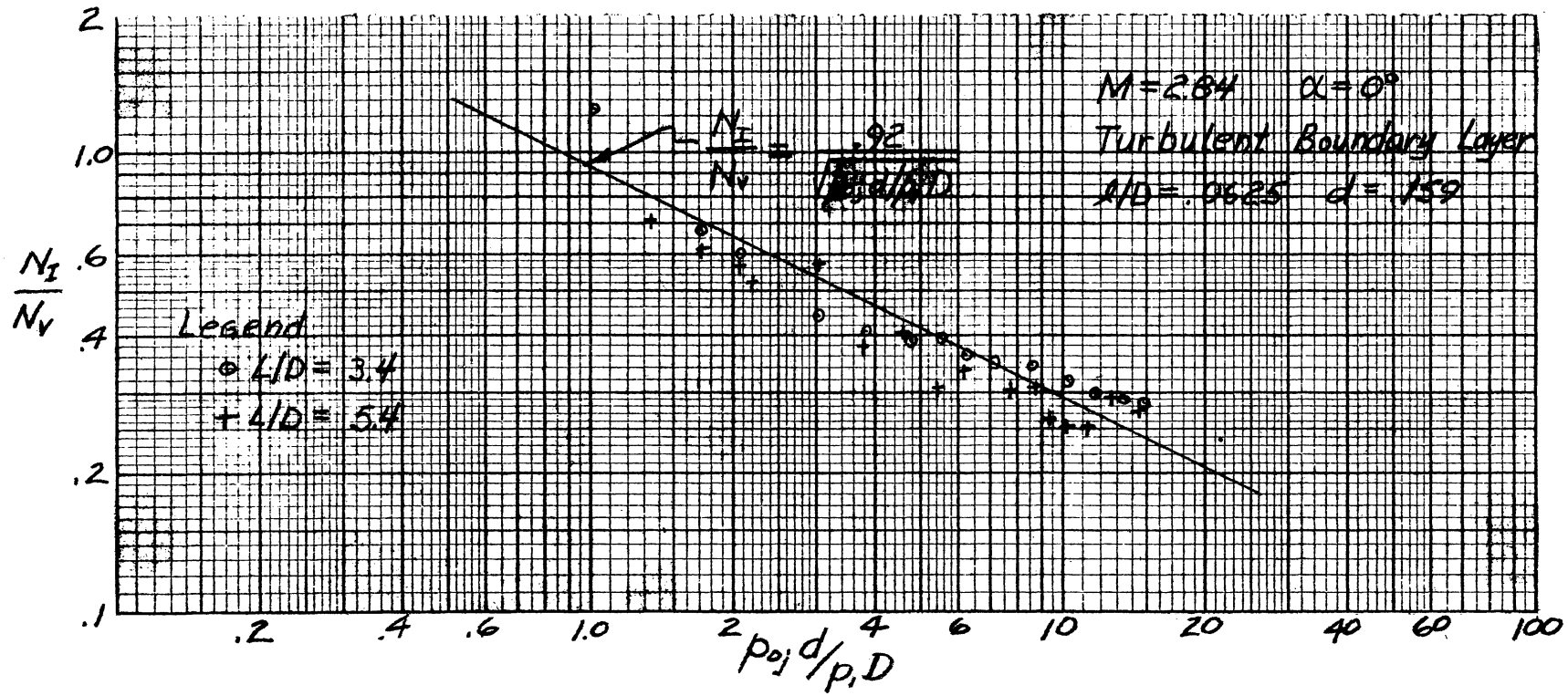

Figure 10. Effect of forebody length on interaction force.

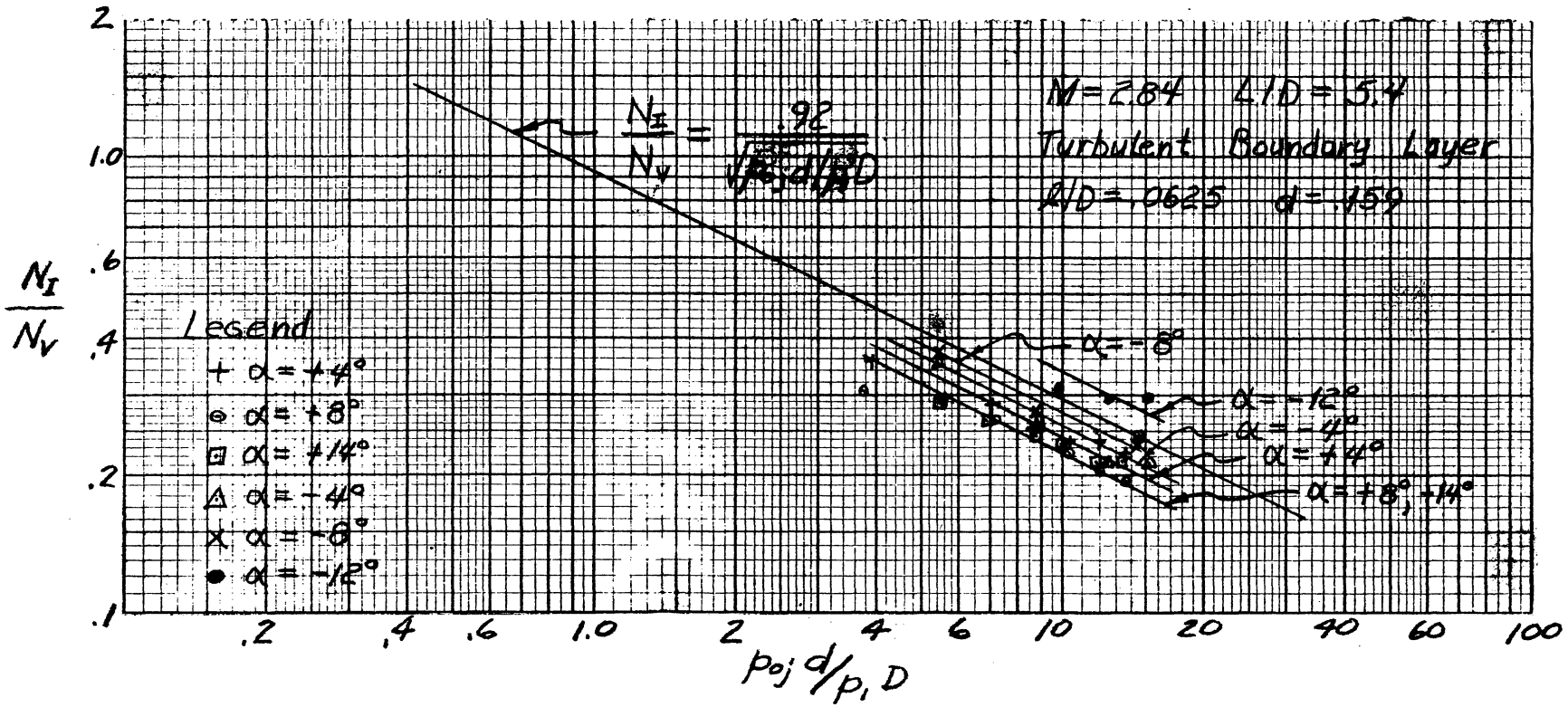

Figure 11. Effect of angle of attack on interaction force.

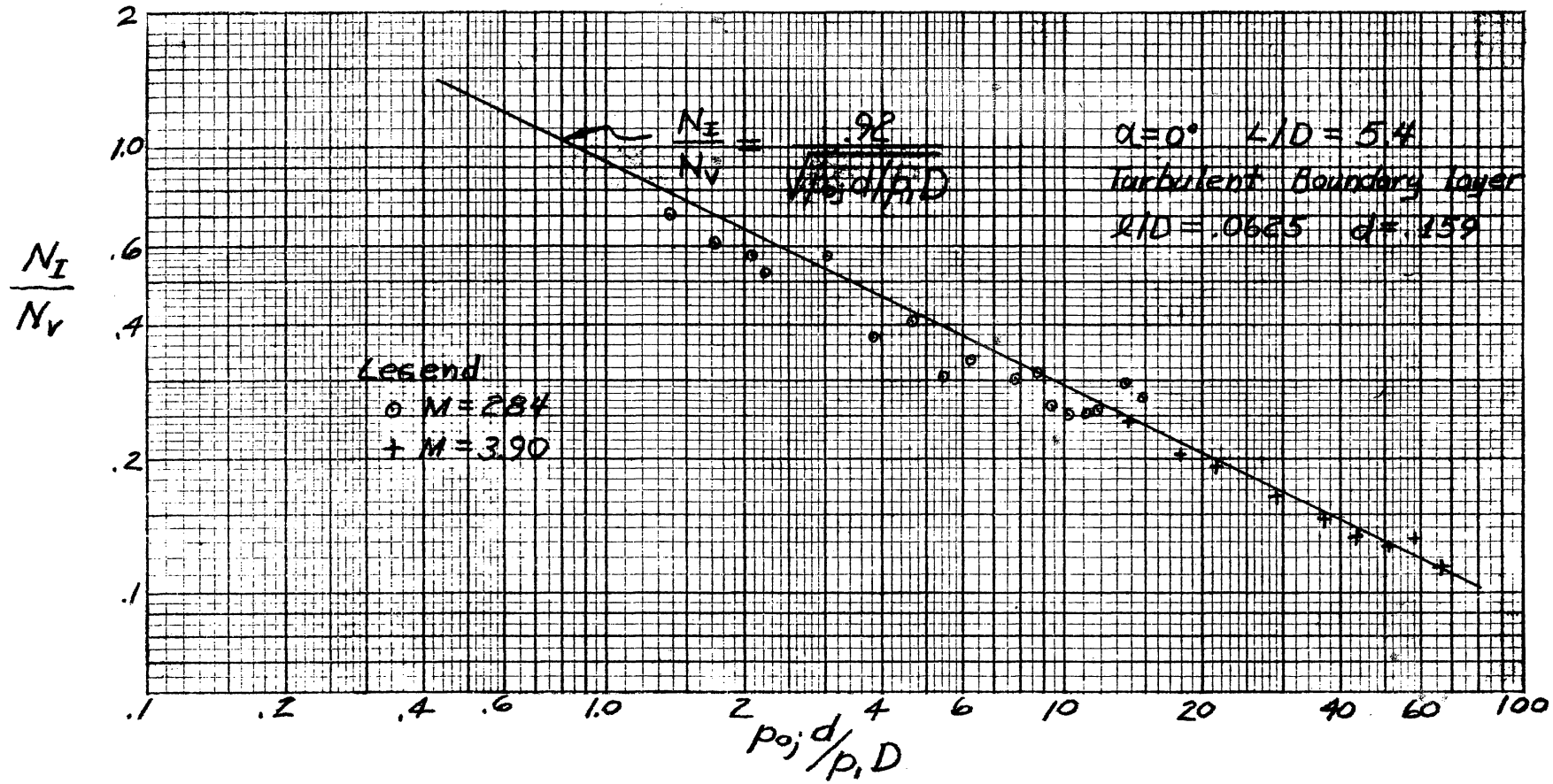

Figure 12. Effect of Mach number on interaction force.

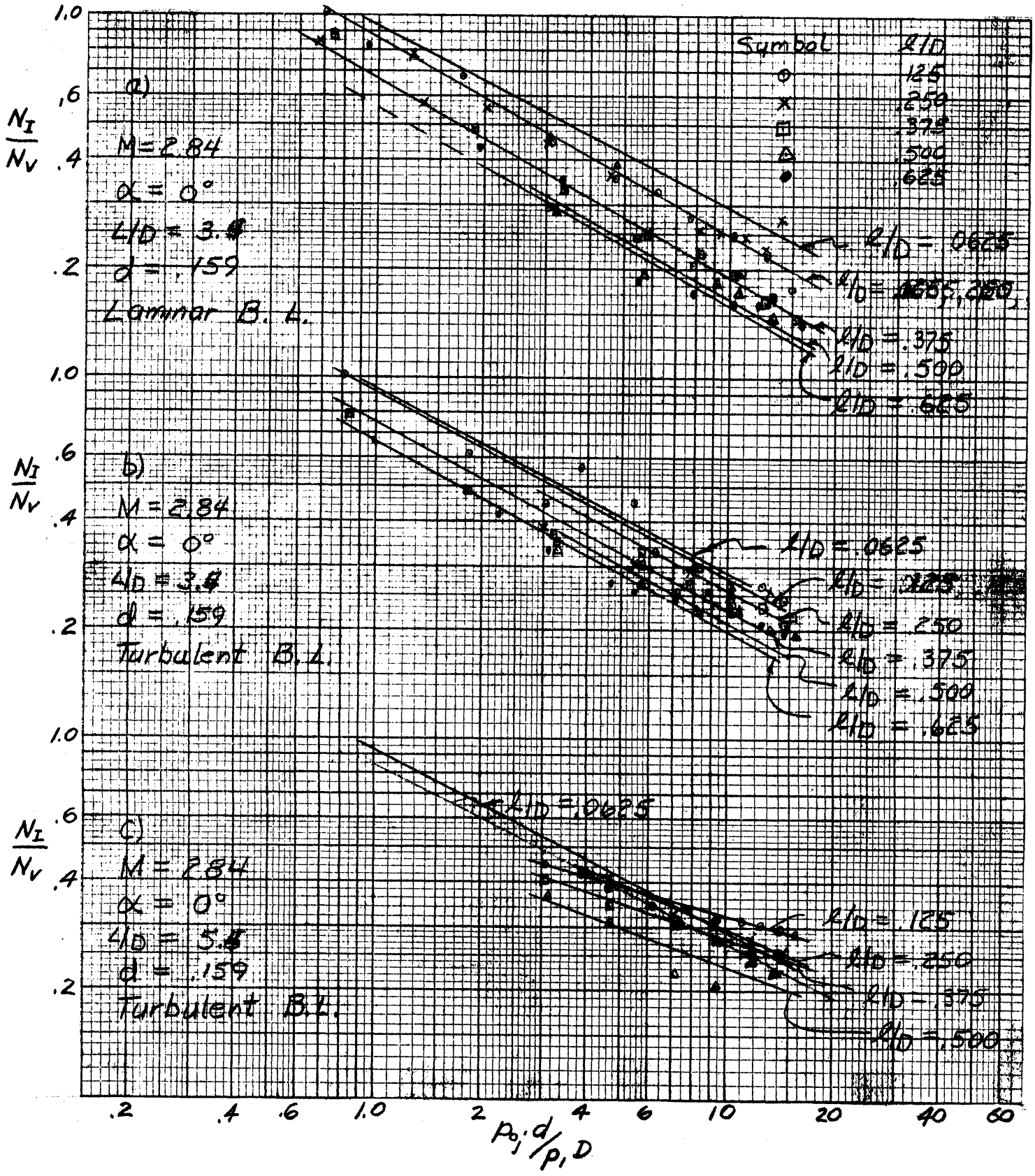

Figure 13. Effect of afterbody length on interaction force.

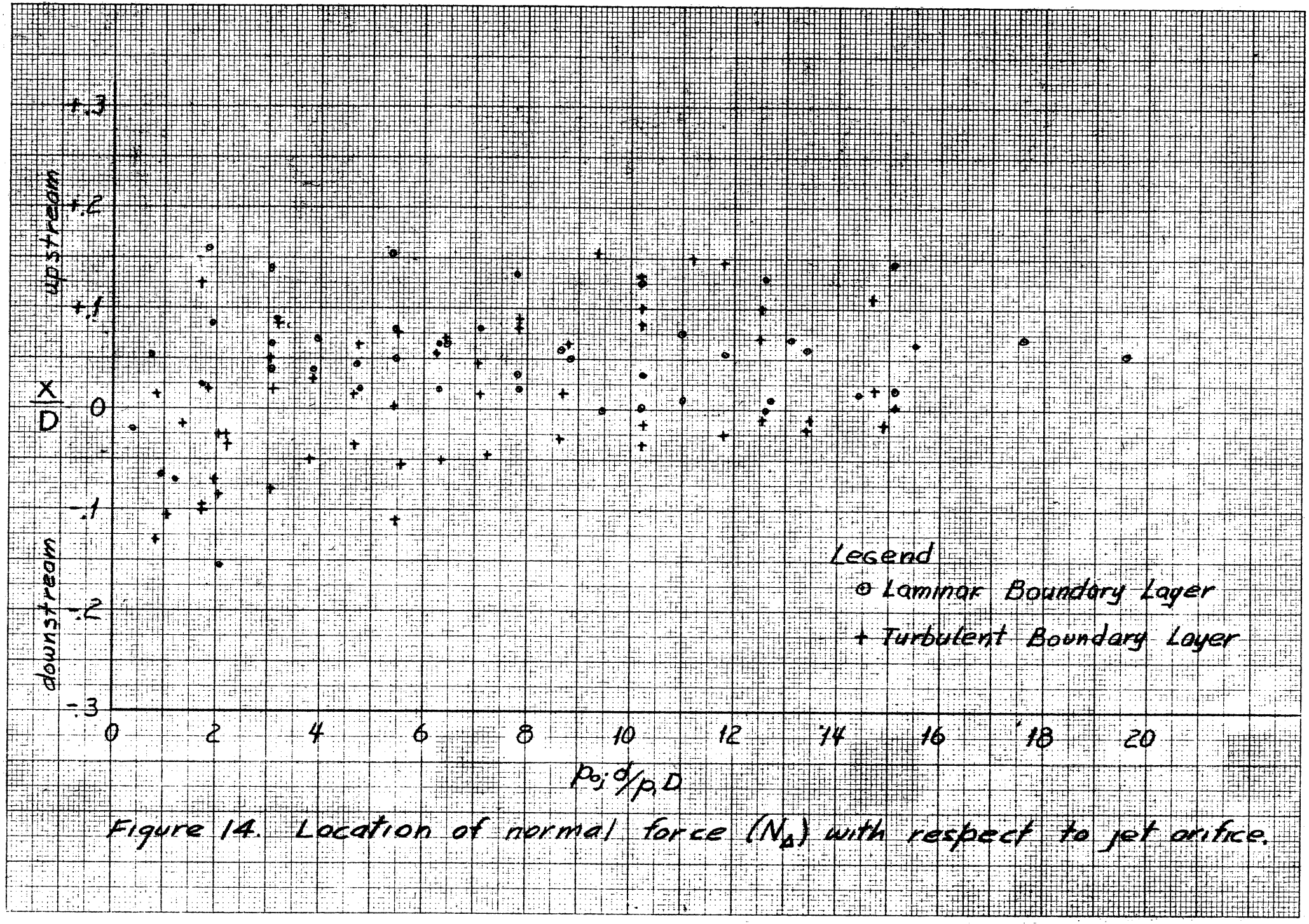

Figure 14. Location of normal force (N_A) with respect to jet orifice.

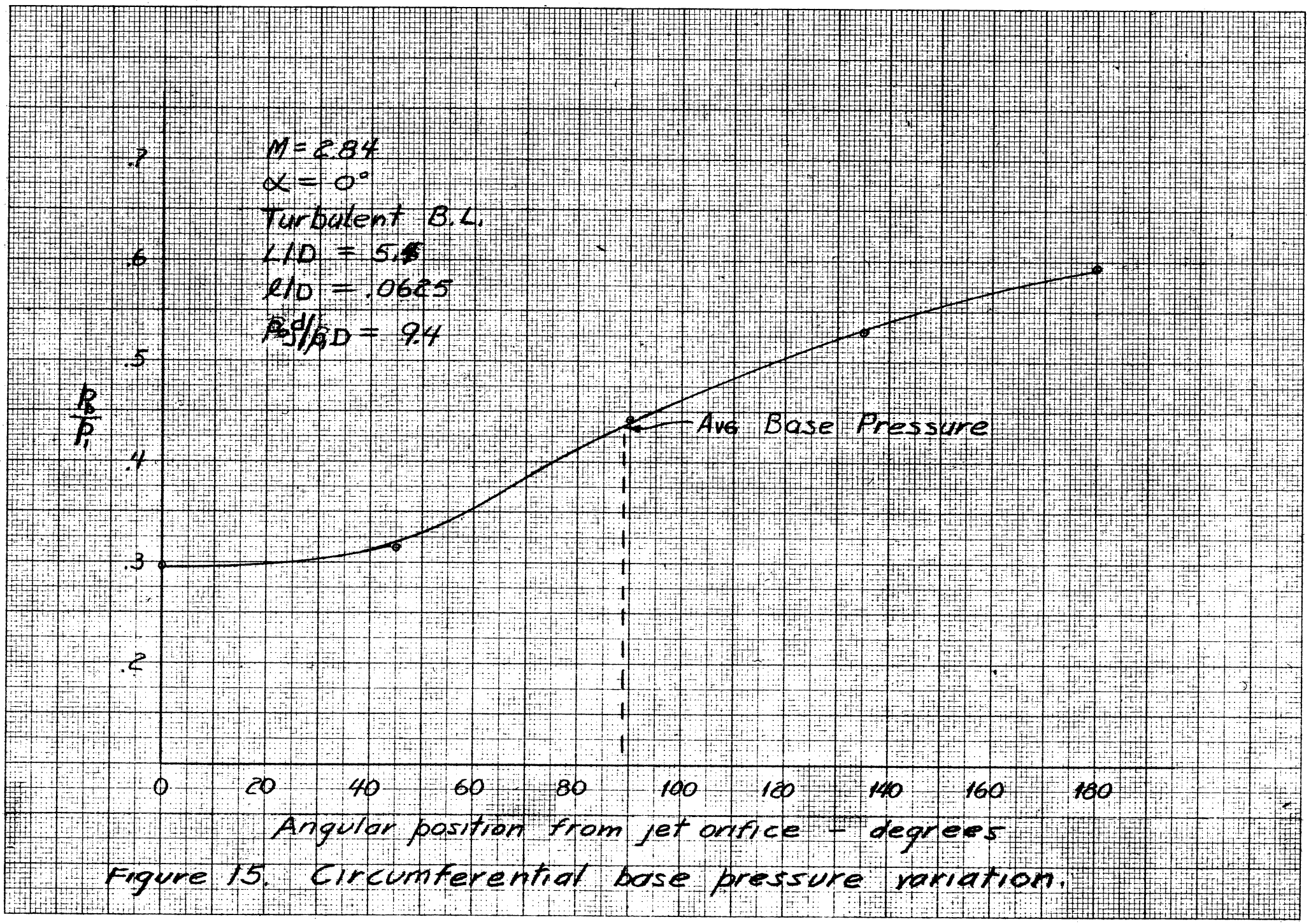

Figure 15. Circumferential base pressure variation.

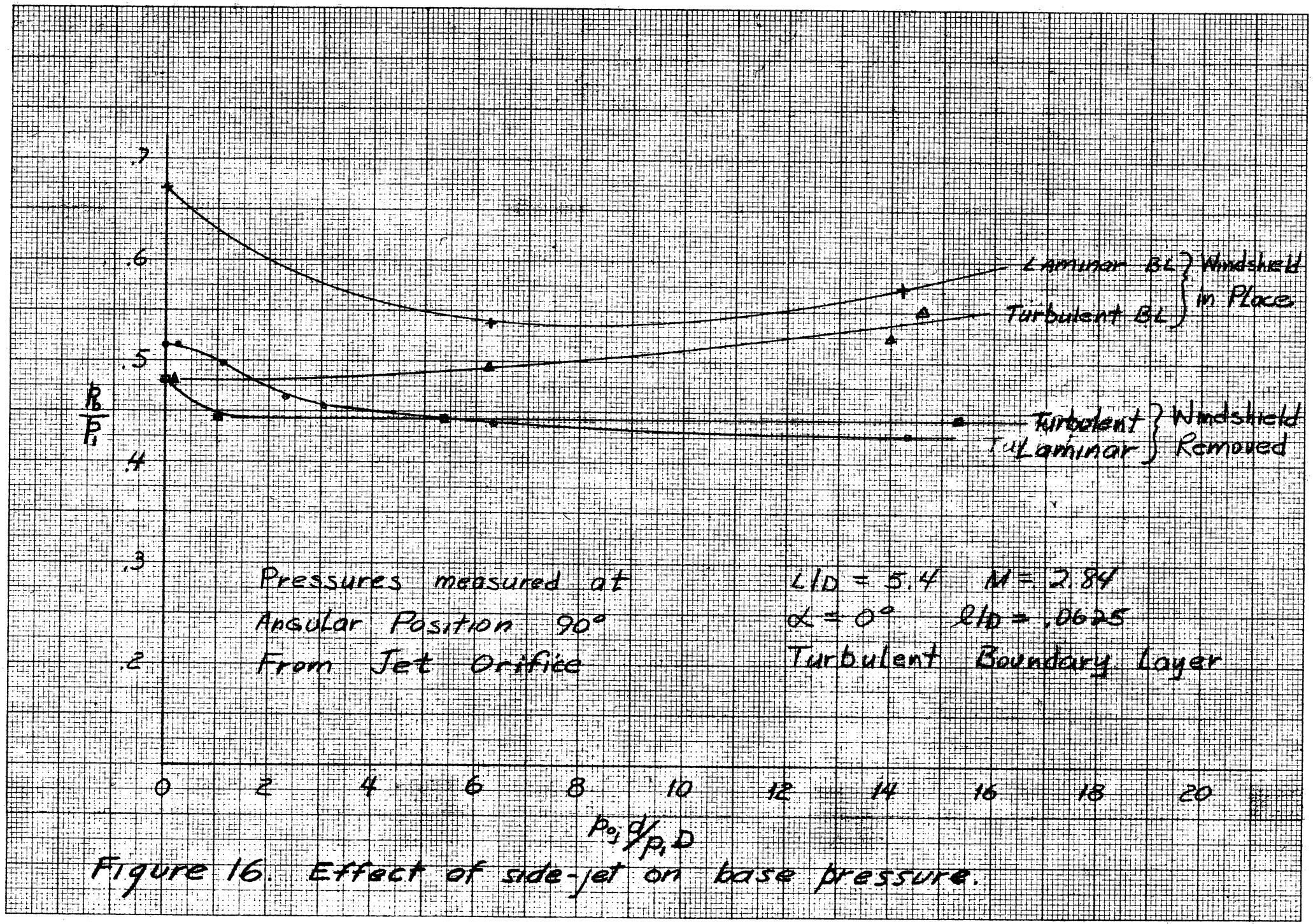

Figure 16. Effect of side-jet on base pressure.

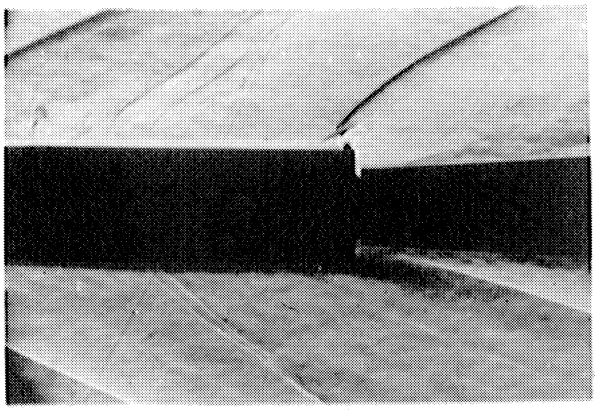

a) $p_{0j}/p_1 = 48$

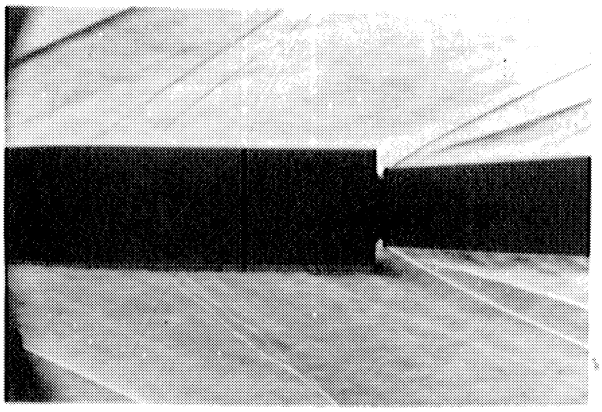

b) $p_{0j}/p_1 = 48$, 90° Roll

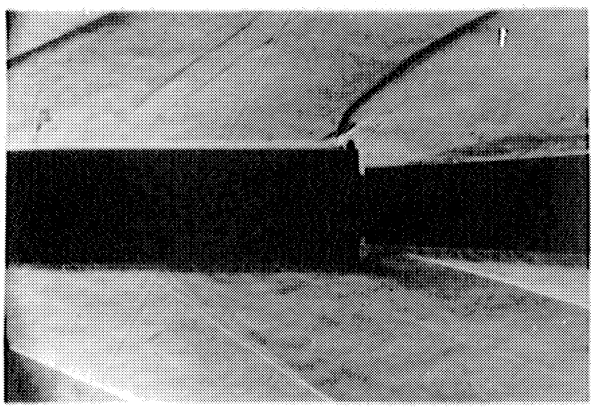

c) $p_{0j}/p_1 = 69$

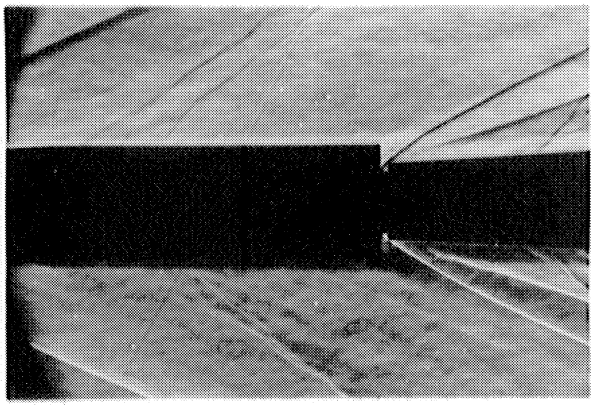

d) $p_{0j}/p_1 = 69$, 90° Roll

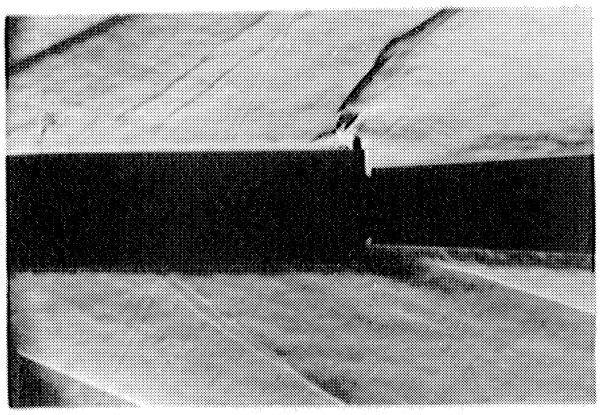

e) $p_{0j}/p_1 = 185$

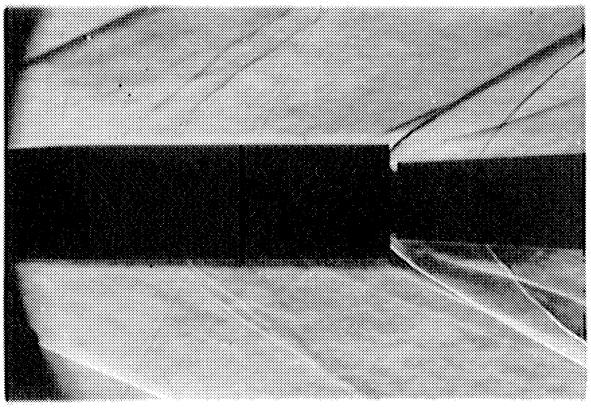

f) $p_{0j}/p_1 = 188$, 90° Roll

Figure 17 Turbulent boundary layer separation ahead of a side-jet, M = 2.84, L/D = 5.4, ℓ/D = .0625, α = 0° d = .159

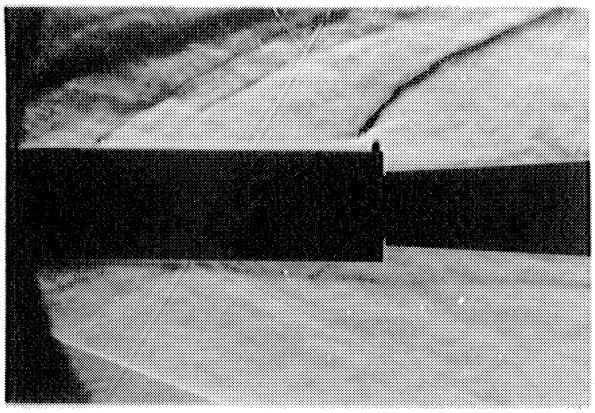

a) $p_{0j}/p_1 = 173$

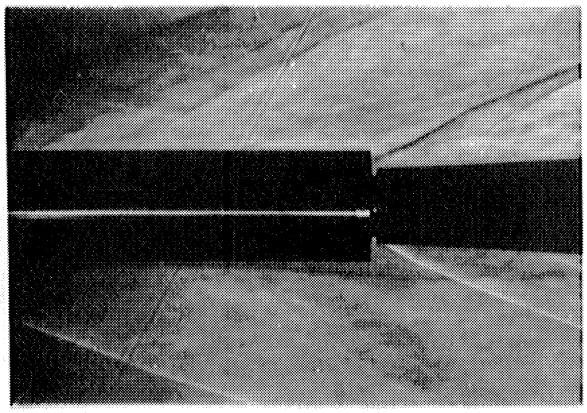

b) $p_{0j}/p_1 = 173$, 90° Roll

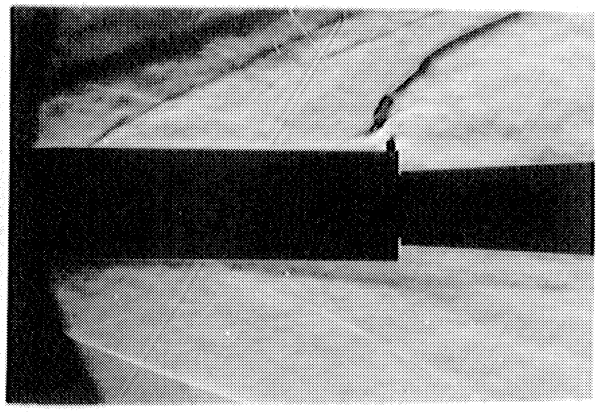

c) $p_{0j}/p_1 = 364$

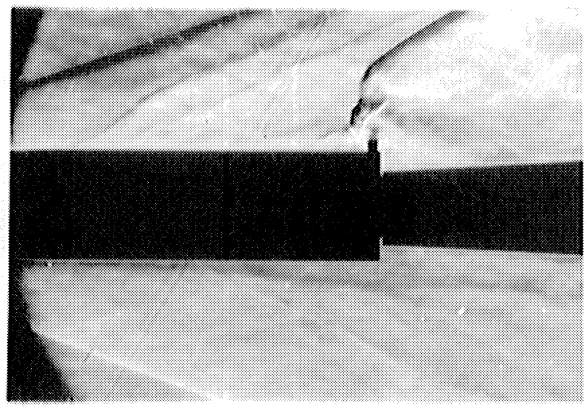

d) $p_{0j}/p_1 = 637$

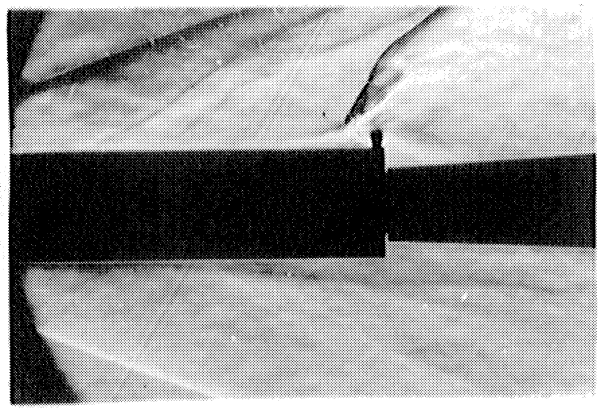

e) $p_{0j}/p_1 = 830$

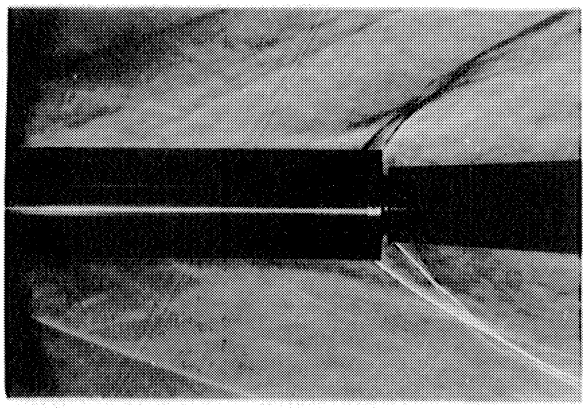

f) $p_{0j}/p_1 = 907$, 90° Roll

Figure 18 Turbulent boundary layer separation ahead of a side-jet, M= 3.90, L/D=5.4, ℓ/D= .0625, α= 0° d= .159

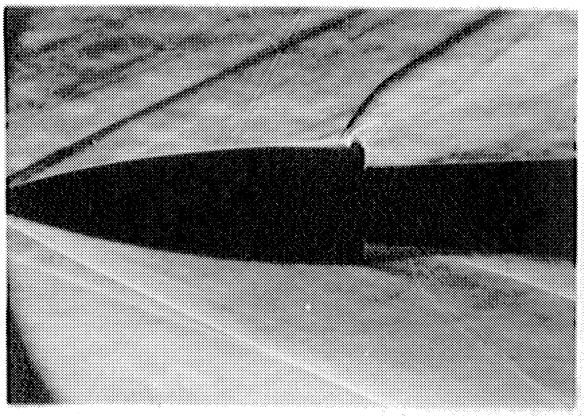

a) $p_{oj}/p_l = 34$, Laminar boundary layer

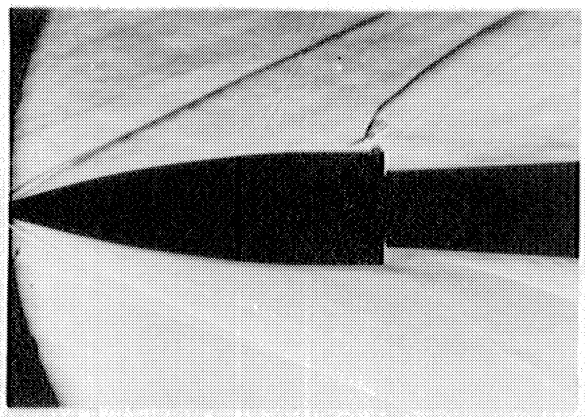

b) $p_{oj}/p_l = 34$, Turbulent boundary layer

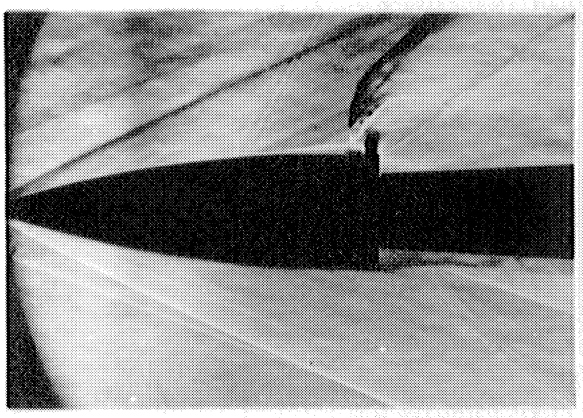

c) $p_{oj}/p_l = 163$, Laminar boundary layer

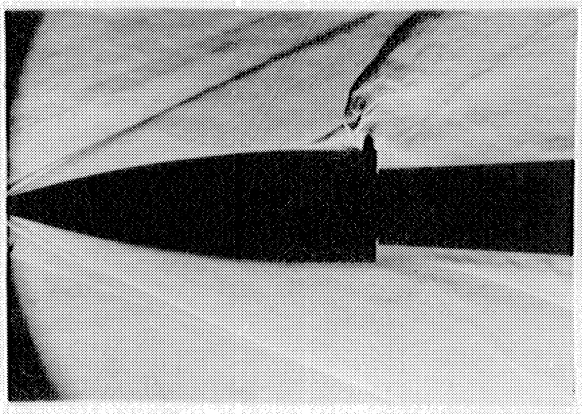

d) $p_{oj}/p_l = 162$, Turbulent boundary layer

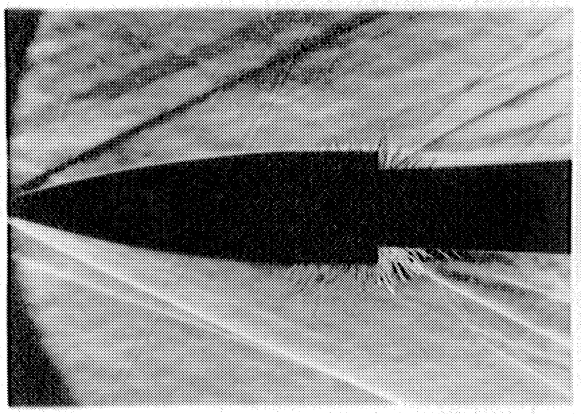

e) $p_{oj}/p_l = 34$, 90° Roll, Laminar boundary layer

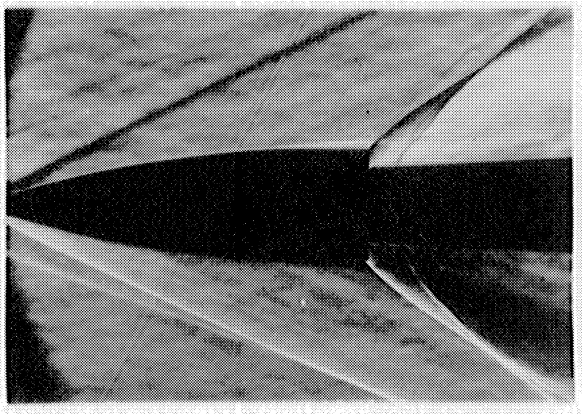

f) $p_{oj}/p_l = 161$, 90° Roll, Laminar boundary layer

Figure 19 Laminar and turbulent separation ahead of a side-jet, $M = 2.84$, $L/D = 3.4$, $\ell/D = .0625$, $\alpha = 0°$, $d = .221$

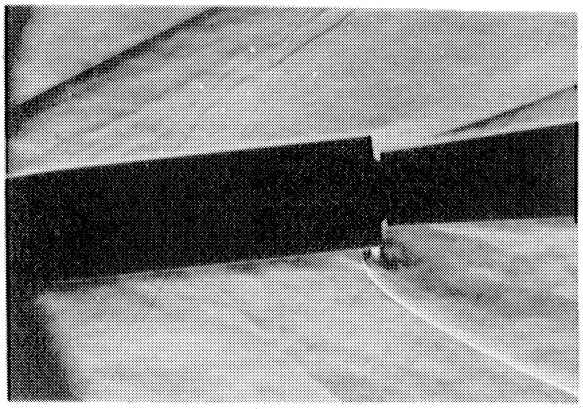

a) $p_{0j}/p_1 = 49$

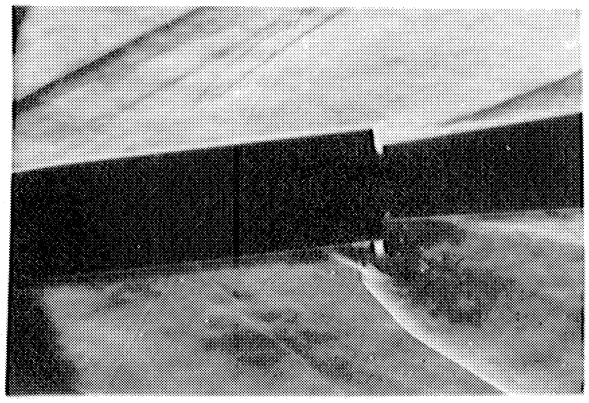

b) $p_{0j}/p_1 = 181$

$\alpha = +5°$

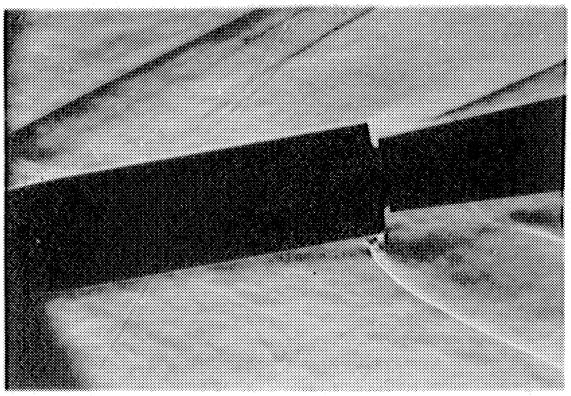

c) $p_{0j}/p_1 = 50$

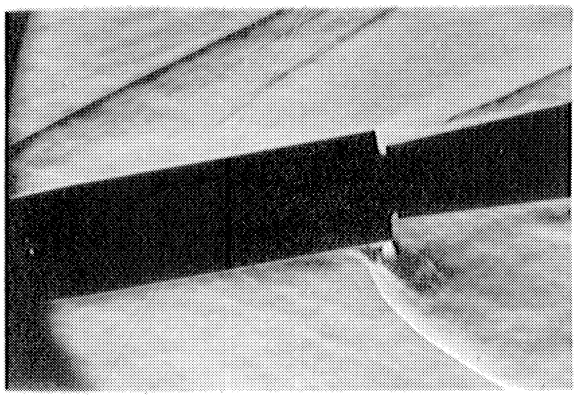

d) $p_{0j}/p_1 = 197$

$\alpha = +10°$

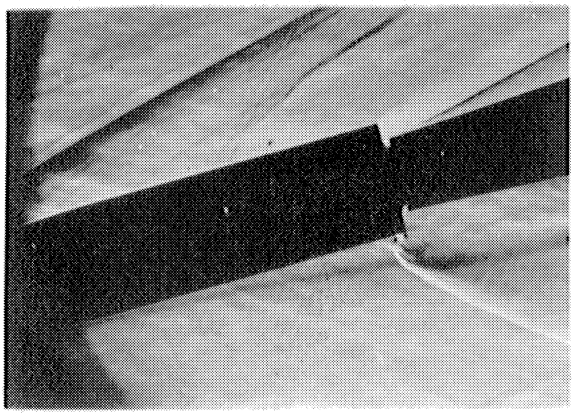

e) $p_{0j}/p_1 = 47$

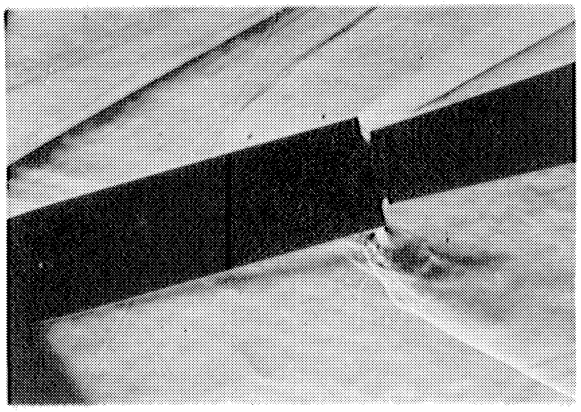

f) $p_{0j}/p_1 = 175$

$\alpha = +14°$

Figure 20 Turbulent separation ahead of a side-jet at positive angles of attack, M = 2.84, L/D = 5.4, δ/D = .0625, d = .159

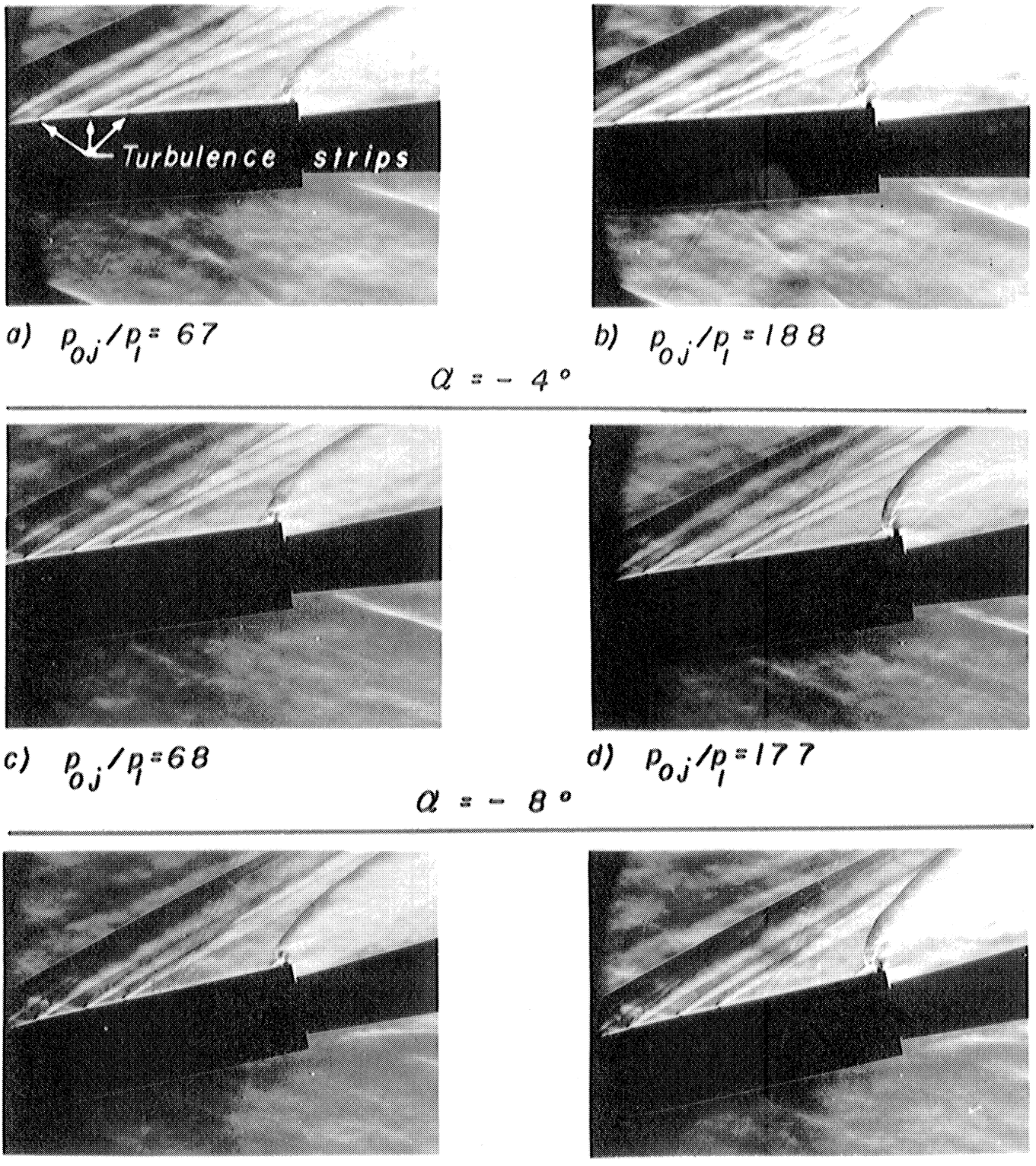

Figure 21 Turbulent separation ahead of a side-jet at negative angles of attack, M = 2.84, L/D = 5.4, ℓ/D = .0625, d = .159

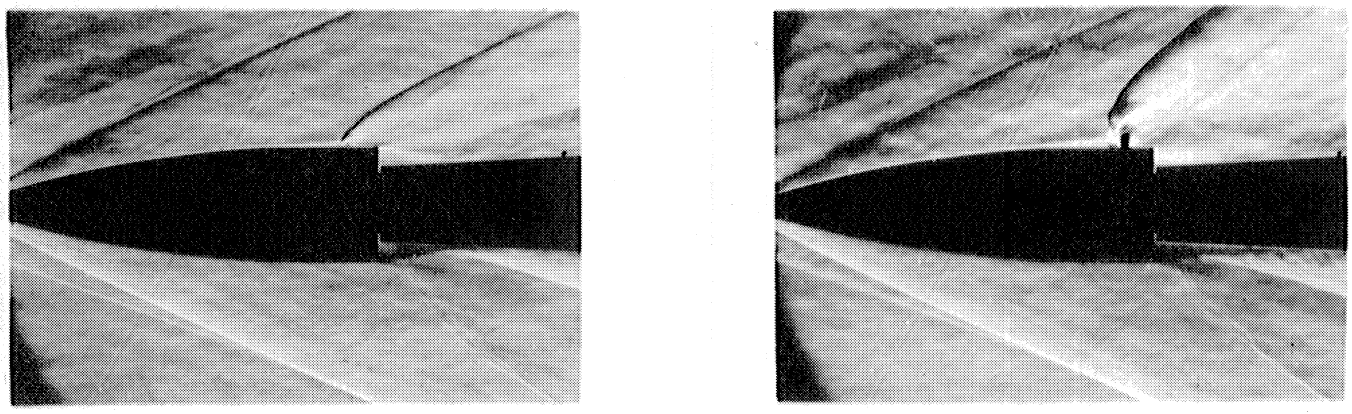

a) $p_{0j}/p_1 = 14$ b) $p_{0j}/p_1 = 160$

$\ell/D = .25$

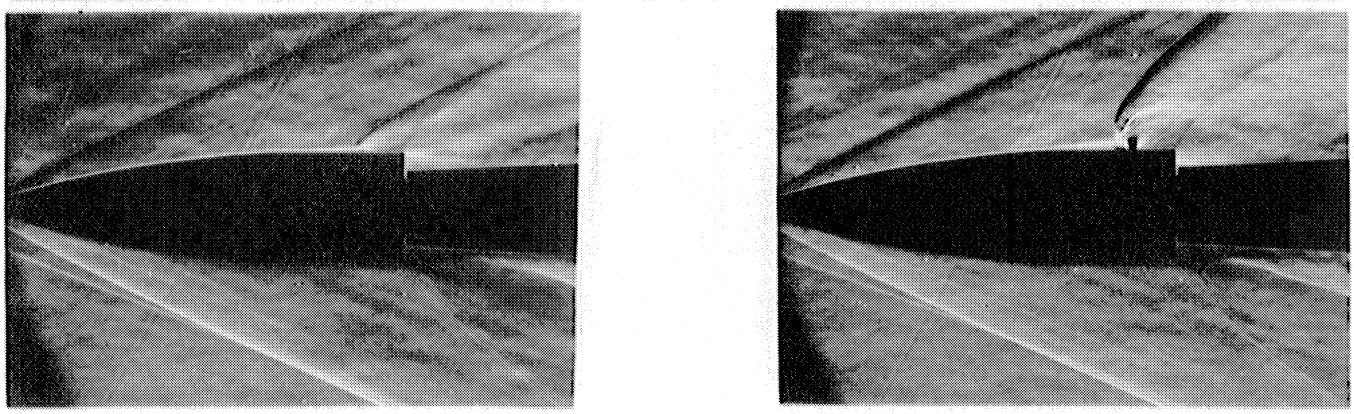

c) $p_{0j}/p_1 = 10$ d) $p_{0j}/p_1 = 173$

$\ell/D = .375$

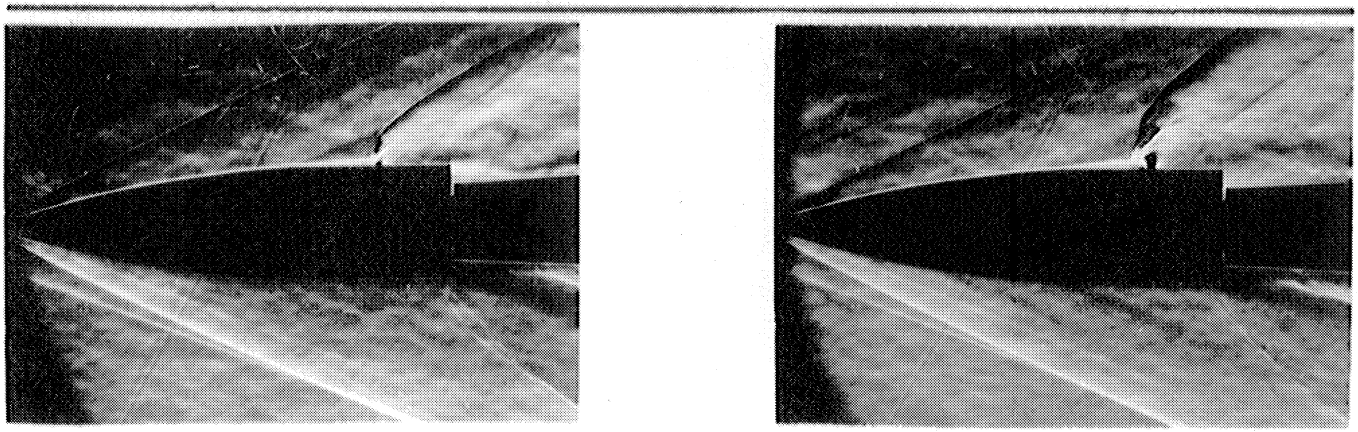

e) $p_{0j}/p_1 = 36$ f) $p_{0j}/p_1 = 173$

$\ell/D = .625$

Figure 22 Laminar separation ahead of a side-jet with various afterbody lengths, $M = 2.84$, $L/D = 3.4$, $\alpha = 0°$, $d = .159$

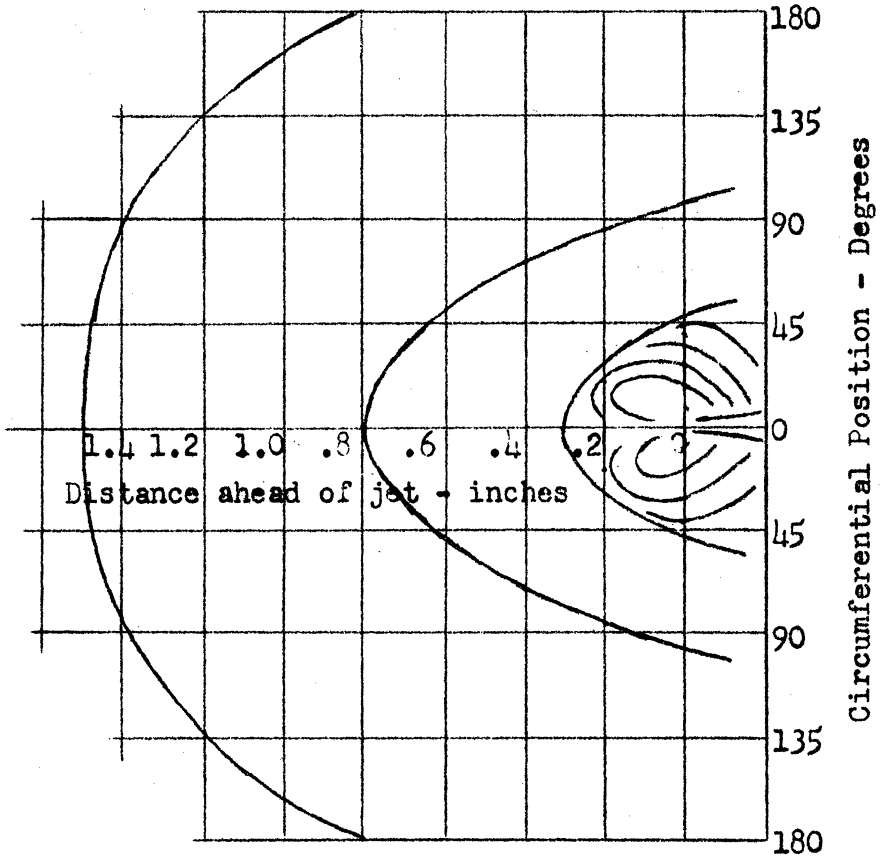

Laminar Boundary Layer

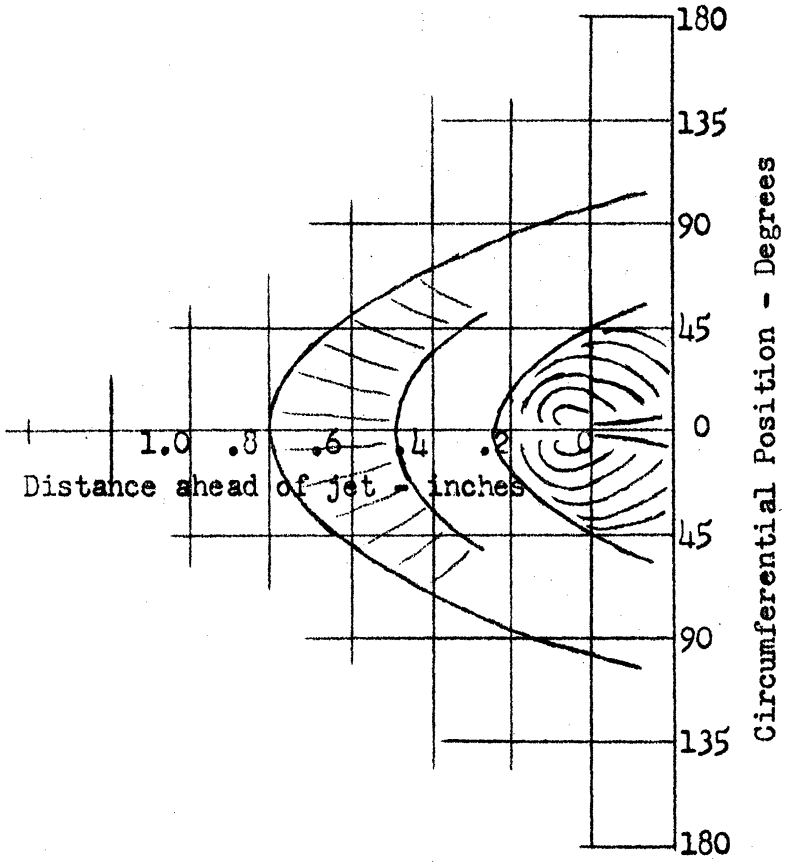

Turbulent Boundary Layer

FIGURE 23. China-clay Patterns of Flow in Vicinity of a Side-jet, p_{oj}/p_1=178 $M = 2.84$, $\alpha = 0°$

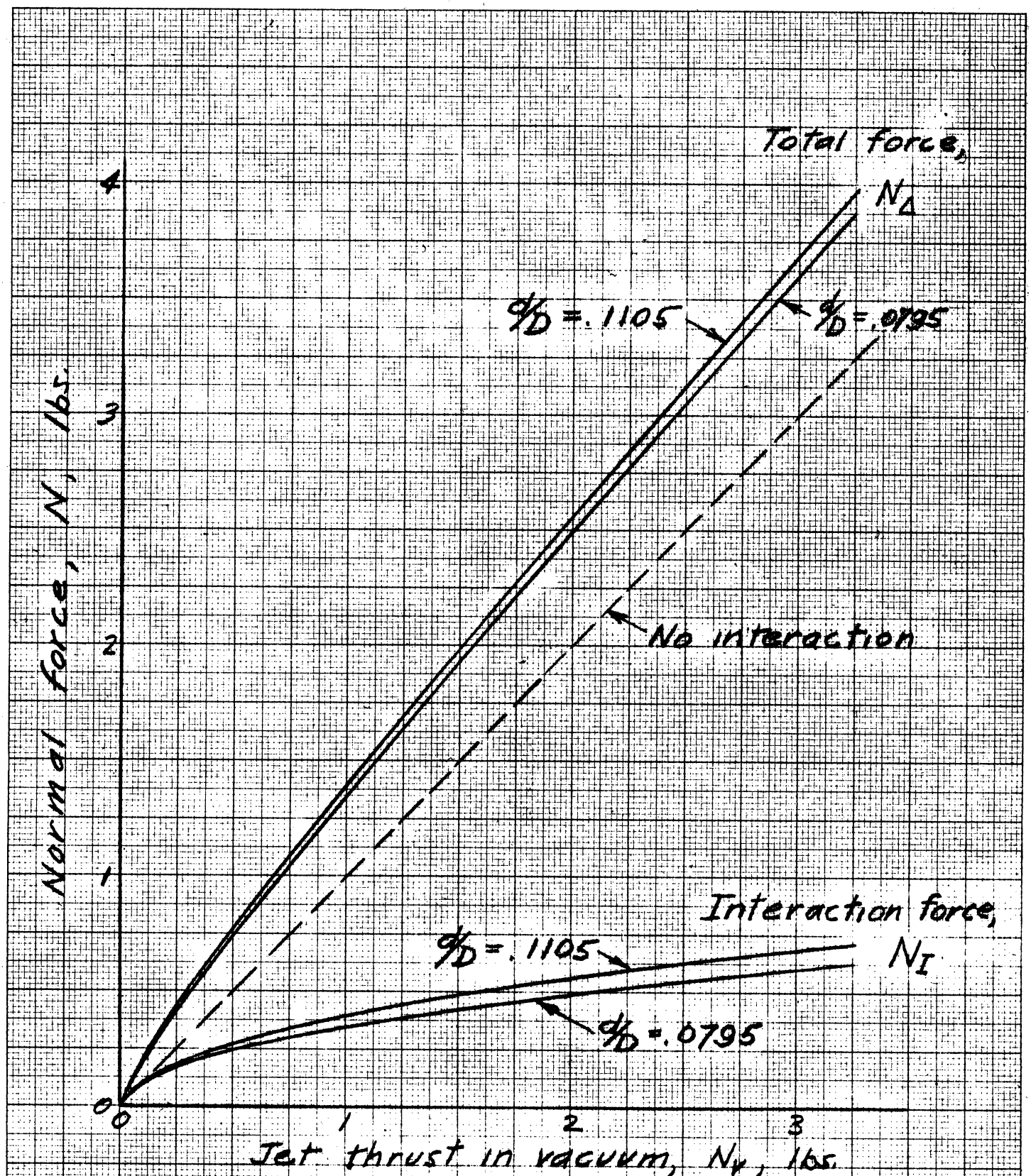

Figure 24. Variation of normal force with jet thrust. p_t = .5 psia, D = 2 inches.